Supporting Information

Influence of Alkali Metal Cations in the Formation of the Heterobimetallic Actinide *tert*-Butoxide $[AnM_3(O^tBu)_7]$ and $[AnM_2(O^tBu)_6]$ (An^{IV} = Th, U; M^I = Li, Na, K, Rb, Cs)

Andreas Lichtenberg,[a] Markus Zegke,[a] Gary S. Nichol,[b] Aida Raauf[,a] and Sanjay Mathur*[,a]*

[a] Institute of Inorganic Chemistry, University of Cologne; 50939 Cologne, Germany

[b] School of Chemistry, The University of Edinburgh, David Brewster Road EH9 3FJ, Edinburgh, Scotland, United Kingdom

*Corresponding Author: aida.raauf@uni-koeln.de; sanjay.mathur@uni-koeln.de

Table of Contents

Crystallography

Table S1 Compiled crystallographic information for the heterobimetallic $Th^{IV}M^I$ *tert*-butoxide compounds **ThLi3**, **ThNa3**, **ThK2**, **ThRb2** and **ThCs2**.

Table S2 Compiled crystallographic information for the heterobimetallic $U^{IV}M^I$ *tert*-butoxide compounds **ULi3**, **UNa2**, **UK2**, **URb2** and **UCs2**.

Table S3 Selected bond lengths and angles for $[AnM_3(O^tBu)_7]$ (**ULi3**, **ThLi3** and **ThNa3**), $[ULi_2(O^tBu)_6(THF)_2]$[20] (**ULi2-THF**), $[U_2Li(O^tBu)_9(THF)]$[20] (**U2Li-THF**) and $[Th_2Na(O^tBu)_9]$[19] (**Th2Na**).

Table S4 Selected bond lengths for $[AnM_2(O^tBu)_6]$ (**UNa2**, **UK2**, **URb2**, **UCs2**, **ThK2**, **ThRb2**, **ThCs2**) and of the reported $[ULi_2(O^tBu)_6(THF_2)]$[20] (**ULi2-THF**).

^{1}H NMR

Figure S1 Paramagnetic ^{1}H NMR spectrum of [$ULi_3(O^tBu)_7$] (**ULi3**) in benzene-d_6 on a 500 MHz *Bruker Avance III 500* spectrometer.

Figure S2 Paramagnetic ^{1}H NMR spectrum of [$ULi_3(O^tBu)_7$] (**ULi3**) in toluene-d_8 on a 500 MHz *Bruker Avance III 500* spectrometer.

Figure S3 Diamagnetic ^{1}H NMR spectrum of [$ThLi_3(O^tBu)_7$] (**ThLi3**) in benzene-d_6 on a 500 MHz *Bruker Avance III 500* spectrometer.

Figure S4 Diamagnetic ^{1}H NMR spectrum of [$ThLi_3(O^tBu)_7$] (**ThLi3**) in toluene-d_8 on a 500 MHz *Bruker Avance III 500* spectrometer.

Figure S5 Diamagnetic ^{1}H NMR spectrum of [$ThNa_3(O^tBu)_7$] (**ThNa3**) in toluene-d_8 on a 500 MHz *Bruker Avance III 500* spectrometer.

Figure S5-a Diamagnetic ^{1}H NMR spectrum of [$ThNa_3(O^tBu)_7$] (**ThNa3**) in toluene-d_8 on a 500 MHz *Bruker Avance III 500* spectrometer at -50 °C (blue) compared with the measurement at room temperature (red).

Figure S6 Paramagnetic ^{1}H NMR spectrum of [$UNa_2(O^tBu)_6$] (**UNa2**) in benzene-d_6 on a 300 MHz *Bruker Avance II 300* spectrometer.

Figure S7 Paramagnetic ^{1}H NMR spectrum of [$UNa_2(O^tBu)_6$] (**UNa2**) in toluene-d_8 on a 500 MHz *Bruker Avance III 500* spectrometer.

Figure S8 Paramagnetic ^{1}H NMR spectrum of [$UK_2(O^tBu)_6$] (**UK2**) in benzene-d_6 on a 300 MHz *Bruker Avance II 300* spectrometer.

Figure S9 Paramagnetic ^{1}H NMR spectrum of [$URb_2(O^tBu)_6$] (**URb2**) in benzene-d_6 on a 300 MHz *Bruker Avance II 300* spectrometer.

Figure S10 Paramagnetic ^{1}H NMR spectrum of [$UCs_2(O^tBu)_6$] (**UCs2**) in benzene-d_6 on a 300 MHz *Bruker Avance II 300* spectrometer.

Figure S11 Diamagnetic ^{1}H NMR spectrum of [$ThK_2(O^tBu)_6$] (**ThK2**) in benzene-d_6 on a 300 MHz *Bruker Avance II 300* spectrometer.

Figure S11-a Variable temperature (rt to -45 °C) 1H NMR of compound **ThK2** in tolouene-d_8 on 500 MHz *Bruker Avance 500* spectrometer.

Figure S12 Diamagnetic ^{1}H NMR spectrum of [$ThRb_2(O^tBu)_6$] (**ThRb2**) in benzene-d_6 on a 300 MHz *Bruker Avance II 300* spectrometer.

Figure S13 Diamagnetic ^{1}H NMR spectrum of [$ThCs_2(O^tBu)_6$] (**ThCs2**) in benzene-d_6 on a 300 MHz *Bruker Avance II 300* spectrometer.

Room temperature alkali metal isotope NMR

Figure S14 Paramagnetic ^{7}Li NMR spectrum of [$ULi_3(O^tBu)_7$] (**ULi3**) in benzene-d_6 on a 300 MHz *Bruker Avance II 300* spectrometer.

Figure S15 Diamagnetic ^{7}Li NMR spectrum of [$ThLi_3(O^tBu)_7$] (**ThLi3**) in benzene-d_6 on a 300 MHz *Bruker Avance II 300* spectrometer.

Figure S16 Diamagnetic ^{23}Na NMR spectrum of [$UTh_3(O^tBu)_7$] (**UTh3**) in toluene-d_8 on a 500 MHz *Bruker Avance 500* spectrometer.

Figure S17 Paramagnetic ^{23}Na NMR spectrum of [$UNa_2(O^tBu)_6$] (**UNa2**) in toluene-d_8 on a 500 MHz *Bruker Avance 500* spectrometer.

Infrared Spectroscopy

Figure S18 Infrared Spectra of the heterobimetallic $Th^{IV}M^{I}$ *tert*-butoxide compounds **ThM3** and **ThM2**

Figure S19 Infrared Spectra of the heterobimetallic $U^{IV}M^{I}$ *tert*-butoxide compounds **UM3** and **UM2**.

Additional Information

Figure S20 Molecular structure of ThK2. The dashed lines emphasize the agostic- and anagostic interactions between the hydrogen atoms of the methyl groups and potassium atoms.

Figure S21 Molecular representation of Th and Na if two distinguishable Na resonances as well as different tBuO resonances were to be seen, which is NOT what we observe (A). In contrast, one single Na resonance indicates that the cubane-type structure (B) is retained even in solution.

Crystallography

Table S1. Compiled crystallographic information for the heterobimetallic $Th^{IV}M^{I}$ *tert*-butoxide compounds **ThLi3**, **ThNa3**, **ThK2**, **ThRb2** and **ThCs2**.

Compound	**ThLi3**	**ThNa3**	**ThK2**	**ThRb2**	**ThCs2**
formula	$ThLi_3O_7C_{28}H_{63}$	$ThNa_3O_7C_{28}H_{63}$	$ThK_2O_6C_{24}H_{54} \cdot C_6H_6$	$ThRb_2O_6C_{24}H_{54} \cdot C_6H_6$	$ThCs_2O_6C_{24}H_{54} \cdot C_6H_6$
CCDC number	2152017	2152018	2152021	2152022	2152020
M_r [g mol^{-1}]	764.65	812.80	827.02	919.76	1014.64
crystal system	trigonal	trigonal	monoclinic	monoclinic	trigonal
space group	*R*3*m*	*R*3*m*	*C*2/*m*	$P2_1/c$	$P3_221$
T [K]	100(2)	100(2)	100(2)	100(2)	100(2)
a [Å]	15.8313(7)	15.7663(4)	12.673(7)	9.7518(4)	10.8621(9)
b [Å]	15.8313(7)	15.7663(4)	16.144(9)	32.6111(15)	10.8621(9)
c [Å]	12.8361(9)	12.9598(5)	9.828(5)	12.7501(6)	28.781(4)
α [°]	90.00	90.00	90.00	90.00	90.00
β [°]	90.00	90.00	110.592(13)	107.336(2)	90.00
γ [°]	120.00	120.00	90.00	90.00	120.00
V [Å^3]	2786.1(3)	2789.90(18)	1882.3(17)	3870.6(3)	2940.8(6)
Z	3	3	2	4	1
μ (M_0-K_α) [mm^{-1}]	3.519	3.512	4.216	6.384	5.666
no. of unique rflns, R_{int}	2465, 0.0866	4948, 0.0491	1796, 0.2425	11788, 0.0547	5439, 0.0493
goodness of fit	1.087	1.135	1.088	1.121	1.348
final *R* indices [$I>2\sigma(I)$]: R_1, wR_2	0.0437, 0.1069	0.0253, 0.0621	0.0817, 0.1881	0.0245, 0.0460	0.0483, 0.1288
R indices (all data): R_1, wR_2	0.0439, 0.1072	0.0253, 0.0621	0.1011, 0.2022	0.0324, 0.0474	0.0484, 0.1288
largest diff. peak and hole	2.88, -1.41	4.38, -1.80	4.44, -2.90	0.67, -1.08	2.97, -4.59

Table S2. Compiled crystallographic information for the heterobimetallic $U^{IV}M^{I}$ *tert*-butoxide compounds **ULi3**, **UNa2**, **UK2**, **URb2** and **UCs2**.

Compound	**ULi3**	**UNa2**	**UK2**	**URb2**	**UCs2**
formula	$ULi_3O_7C_{28}H_{63}$	$UNa_2O_6C_{24}H_{54} \cdot C_6H_6$	$UK_2O_6C_{24}H_{54} \cdot C_6H_6$	$URb_2O_6C_{24}H_{54} \cdot C_6H_6$	$UCs_2O_6C_{24}H_{54} \cdot 1.5\ C_6H_6$
CCDC number	2152019	2152025	2152024	2152026	2152023
M_r [g mol^{-1}]	770.61	800.79	833.01	925.75	1059.68
crystal system	trigonal	orthorhombic	monoclinic	monoclinic	monoclinic
space group	*R*3*m*	*Pnma*	$P2_1/m$	*Cm*	$P2_1/c$
T [K]	100(2)	100(2)	100(2)	100(2)	100(2)
a [Å]	15.7163(6)	20.0126(17)	9.7346(5)	12.6473(15)	21.485(4)
b [Å]	15.7163(6)	16.6888(13)	16.0792(8)	48.949(6)	10.8929(16)
c [Å]	12.7595(6)	12.6265(11)	12.6082(7)	9.7402(12)	18.197(3)
α [°]	90.00	90.00	90.00	90.00	90.00
β [°]	90.00	90.00	110.060(2)	107.407(4)	106.049(6)
γ [°]	120.00	90.00	90.00	90.00	90.00
V [Å^3]	2729.4(2)	4217.1(6)	1853.77(17)	5753.7(12)	4092.7(11)
Z	3	4	2	6	4
μ (M_0-K_α) [mm^{-1}]	4.495	3.366	4.637	6.786	5.754
no. of unique rflns, R_{int}	1385, 0.0575	7884, 0.0774	8015, 0.0866	18481, 0.0742	7469, 0.0915
goodness of fit	1.084	1.282	1.086	1.165	1.111
final *R* indices [$I>2\sigma(I)$]: R_1, wR_2	0.0101, 0.0239	0.0433, 0.0936	0.0462, 0.1260	0.0633, 0.1478	0.0445, 0.0930
R indices (all data): R_1, wR_2	0.0101, 0.0239	0.0497, 0.0963	0.0598, 0.1320	0.0635, 0.1479	0.0569, 0.1002
largest diff. peak and hole	0.21, -0.20	1.80, -2.87	3.68, -5.59	8.28, -13.46	2.21, -1.73

Table S3. Selected bond lengths and angles for $[AnM_3(O^tBu)_7]$ (**ULi3**, **ThLi3** and **ThNa3**), $[ULi_2(O^tBu)_6(THF)_2]$[20] (**ULi2-THF**), $[U_2Li(O^tBu)_9(THF)]$[20] (**U2Li-THF**) and $[Th_2Na(O^tBu)_9]$[19] (**Th2Na**).

Compound	**ULi3**	**ThLi3**	**ThNa3**	**ULi2-THF**	**U2Li-THF**	**Th2Na**
An – M [Å]	3.243(7)	3.299(23)	3.606(3)	2.879(16)	2.927	3.379
M – M [Å]	2.460(9)	2.432(25)	3.091(3)	2.89(3)	-	-
M – $O_{\mu3}1$ [Å]	1.901(8)	1.860(30)	2.234(5)	-	-	-
M – $O_{\mu3}2$ [Å]	1.945(6)	1.990(19)	2.296(4)	1.990(17)	2.058	2.400
An – $O_{\mu3}2$ [Å]	2.385(3)	2.403(8)	2.425(4)	2.398(9)	2.494	2.483
An – O_t [Å]	2.120(3)	2.193(6)	2.190(4)	2.139(9)	2.114	2.155
O_t – An – $O_{\mu3}2$ (trans) [°]	162.98(9)	163.0(3)	166.6(1)			

Table S4. Selected bond lengths for $[AnM_2(O^tBu)_6]$ (**UNa2**, **UK2**, **URb2**, **UCs2**, **ThK2**, **ThRb2**, **ThCs2**) and of the reported $[ULi_2(O^tBu)_6(THF_2)]$[20] (**ULi2-THF**).

Compound	**ULi2-THF**[1]	**UNa2**	**UK2**	**URb2**	**UCs2**
M – $O_{\mu2}$ [Å]	2.045(18)	2.321(4)	2.642(6)	2.768(13)	2.932(6)
M – $O_{\mu3}$ [Å]	1.990(17)	2.329(3)	2.665(4)	2.791(13)	2.989(6)
An – $O_{\mu2}$ [Å]	2.252(6)	2.249(3)	2.232(5)	2.242(12)	2.262(6)
An – $O_{\mu3}$ [Å]	2.398(9)	2.398(4)	2.337(3)	2.347(13)	2.326(6)
An – O_t [Å]	2.139(9)	2.145(4)	2.169(3)	2.181(12)	2.173(6)
Compound	**ThK2**	**ThRb2**	**ThCs2**		
M – $O_{\mu2}$ [Å]	3.060(30)	2.779(3)	2.995(11)		
M – $O_{\mu3}$ [Å]	2.879(17)	2.802(3)	2.995(10)		
An – $O_{\mu2}$ [Å]	2.268(19)	2.287(2)	2.319(9)		
An – $O_{\mu3}$ [Å]	2.301(13)	2.397(3)	2.390(9)		
An – O_t [Å]	-	2.223(3)	2.214(9)		

Room temperature ^{1}H NMR

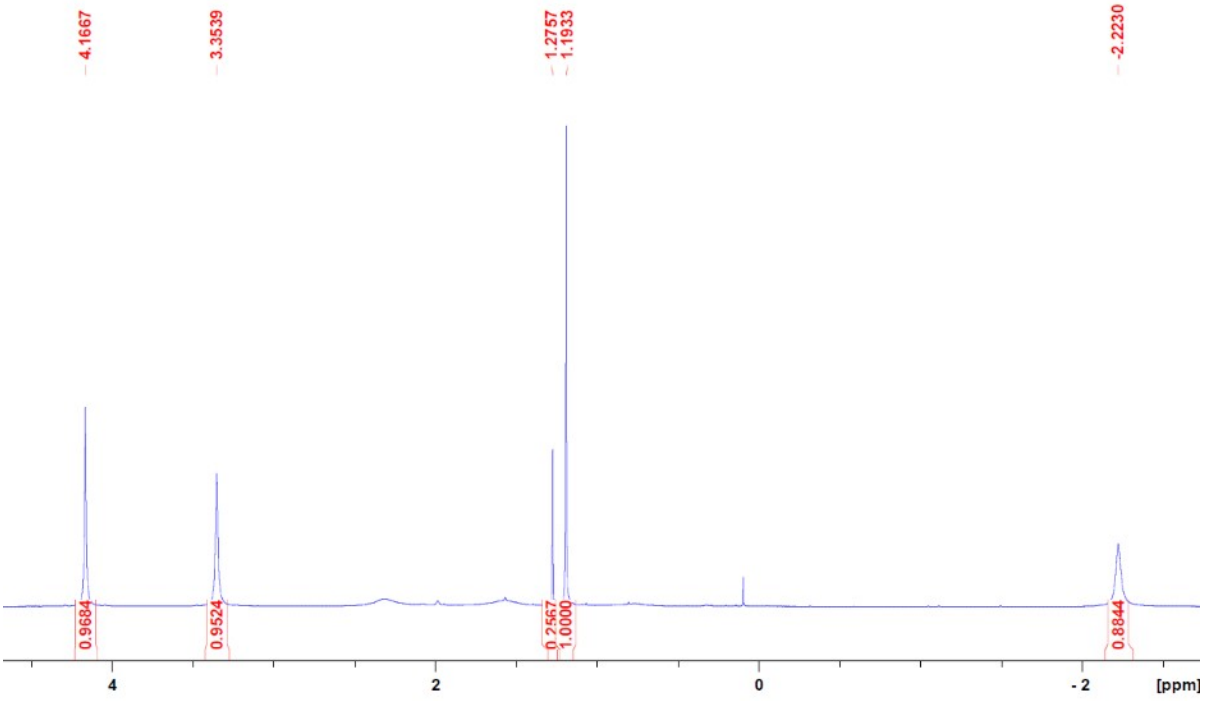

Figure S1 Paramagnetic ^{1}H NMR spectrum of $[ULi_3(O^tBu)_7]$ (**ULi3**) in benzene-d_6 on a 500 MHz *Bruker Avance III 500* spectrometer.

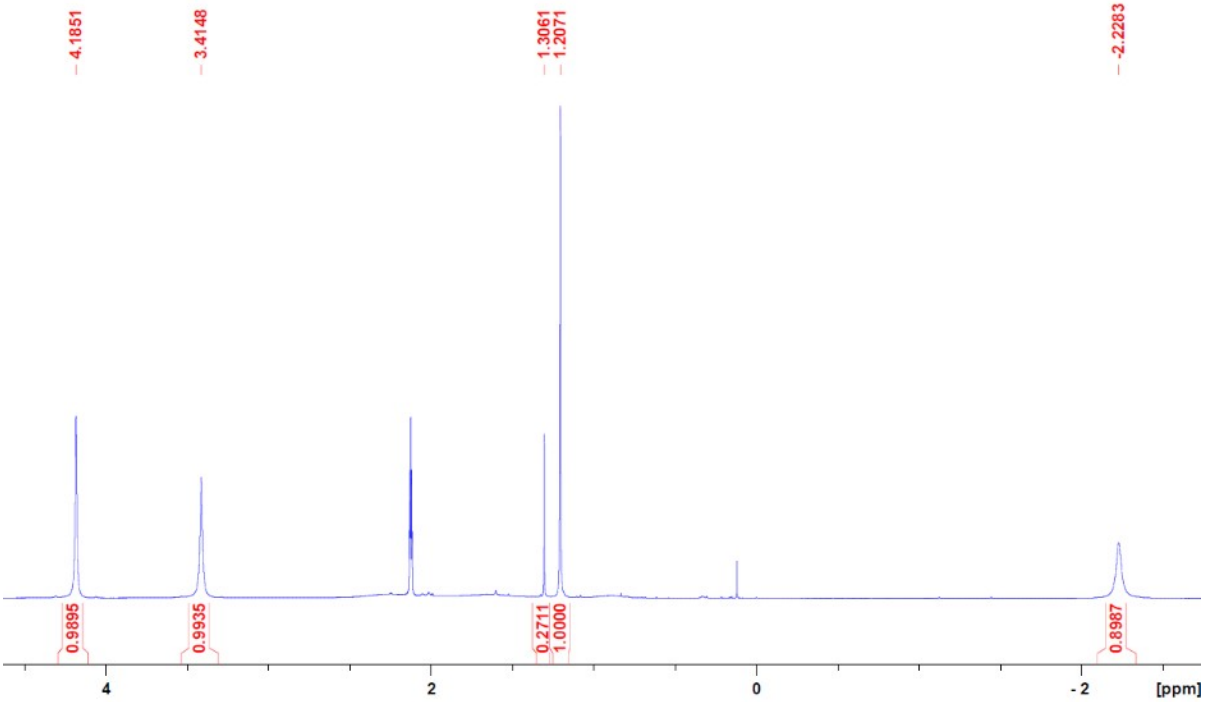

Figure S2 Paramagnetic ^{1}H NMR spectrum of $[ULi_3(O^tBu)_7]$ (**ULi3**) in toluene-d_8 on a 500 MHz *Bruker Avance III 500* spectrometer.

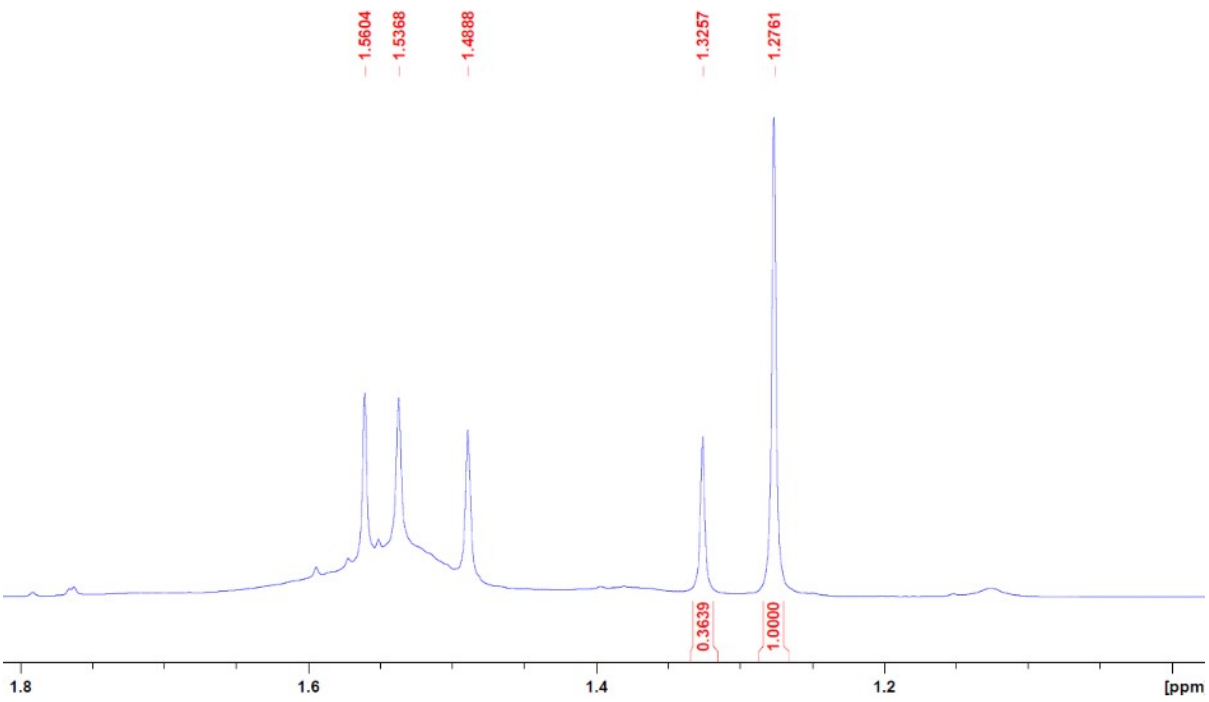

Figure S3 Diamagnetic ^{1}H NMR spectrum of [$ThLi_3(O^tBu)_7$] (**ThLi3**) in benzene-d_6 on a 500 MHz *Bruker Avance III 500* spectrometer.

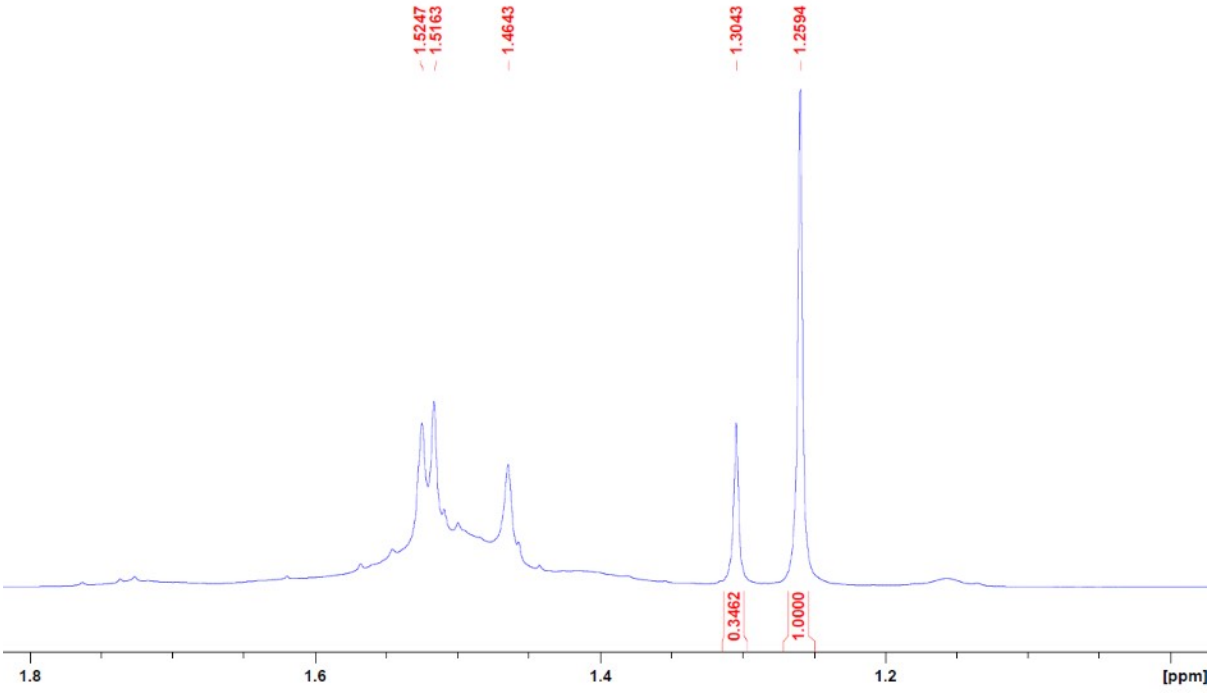

Figure S4 Diamagnetic ^{1}H NMR spectrum of [$ThLi_3(O^tBu)_7$] (**ThLi3**) in toluene-d_8 on a 500 MHz *Bruker Avance III 500* spectrometer.

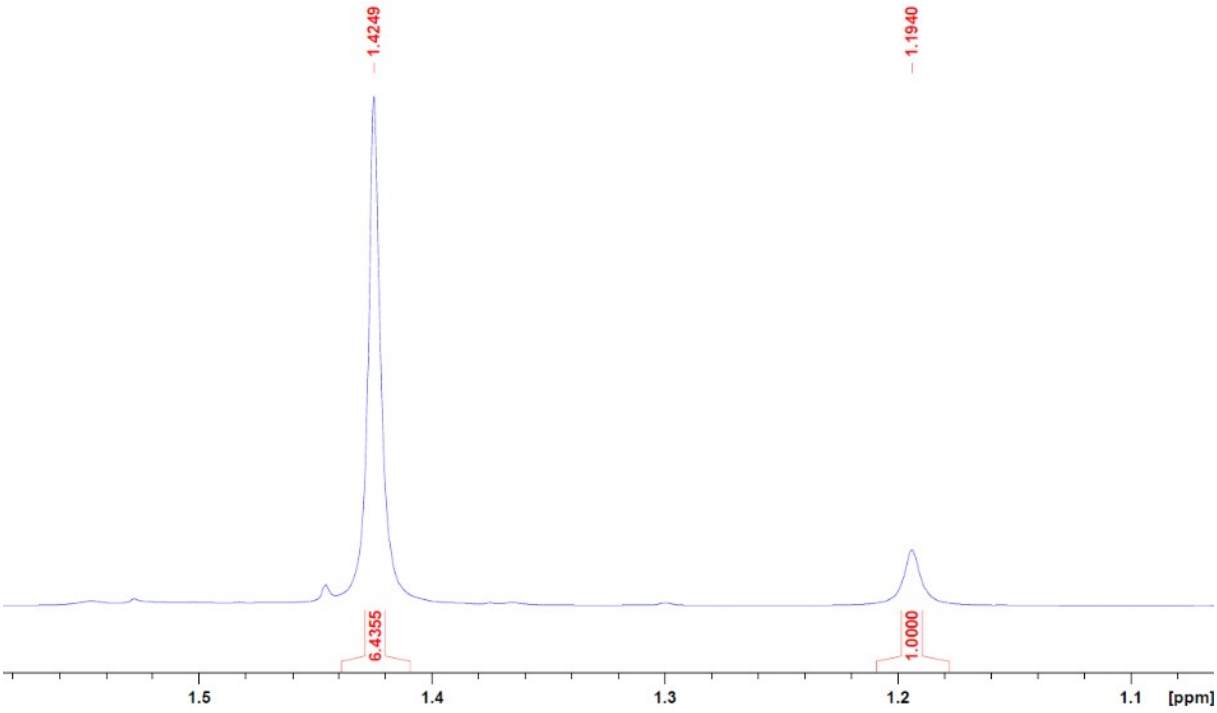

Figure S5 Diamagnetic ^{1}H NMR spectrum of [ThNa$_3$(O^{t}Bu)$_7$] (**ThNa3**) in toluene-d_8 on a 500 MHz *Bruker Avance III 500* spectrometer.

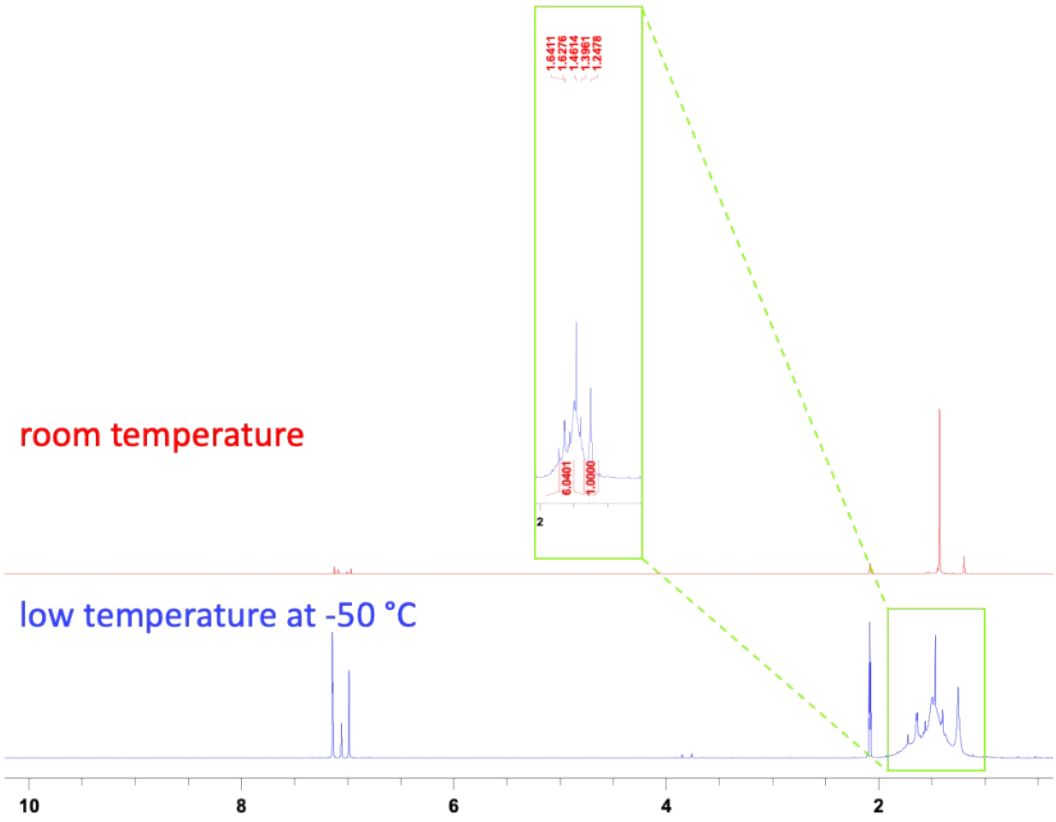

S5-a Diamagnetic ^{1}H NMR spectrum of [ThNa$_3$(O^{t}Bu)$_7$] (**ThNa3**) in toluene-d_8 on a 500 MHz *Bruker Avance III 500* spectrometer at -50 °C (blue) compared with the measurement at room temperature (red).

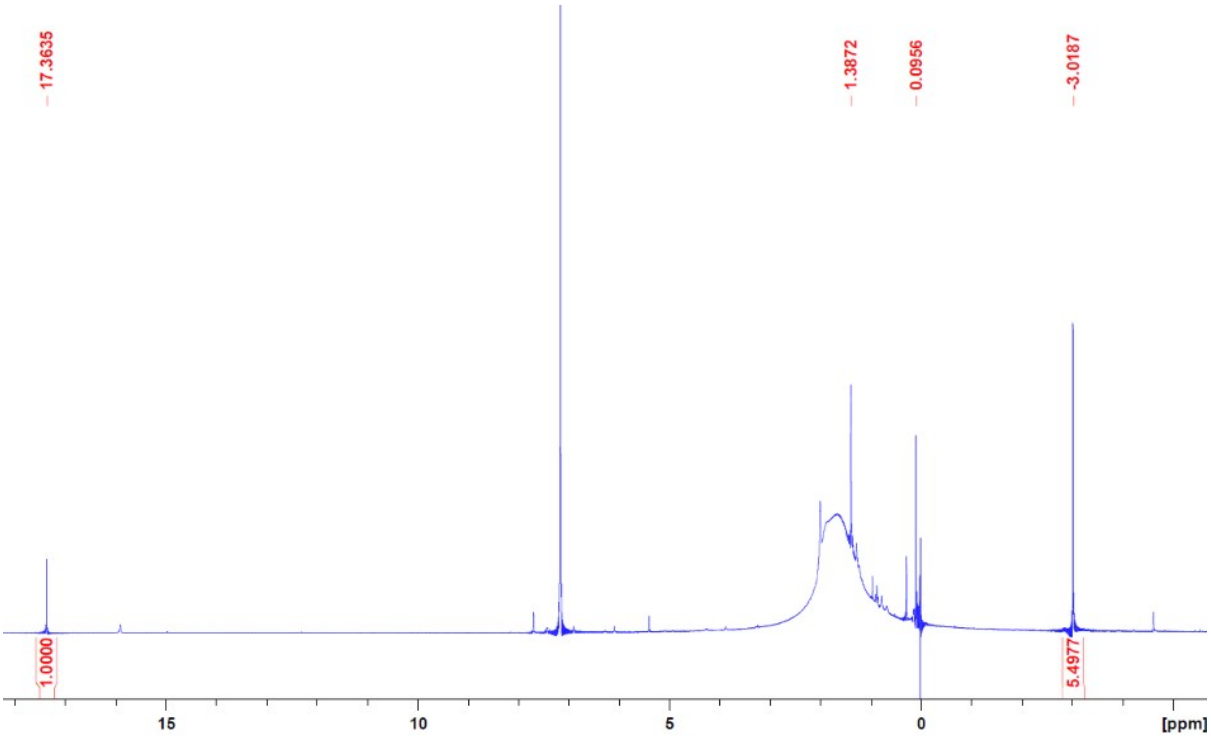

Figure S6 Paramagnetic ^{1}H NMR spectrum of [$UNa_2(O^tBu)_6$] (**UNa2**) in benzene-d_6 on a 300 MHz *Bruker Avance II 300* spectrometer.

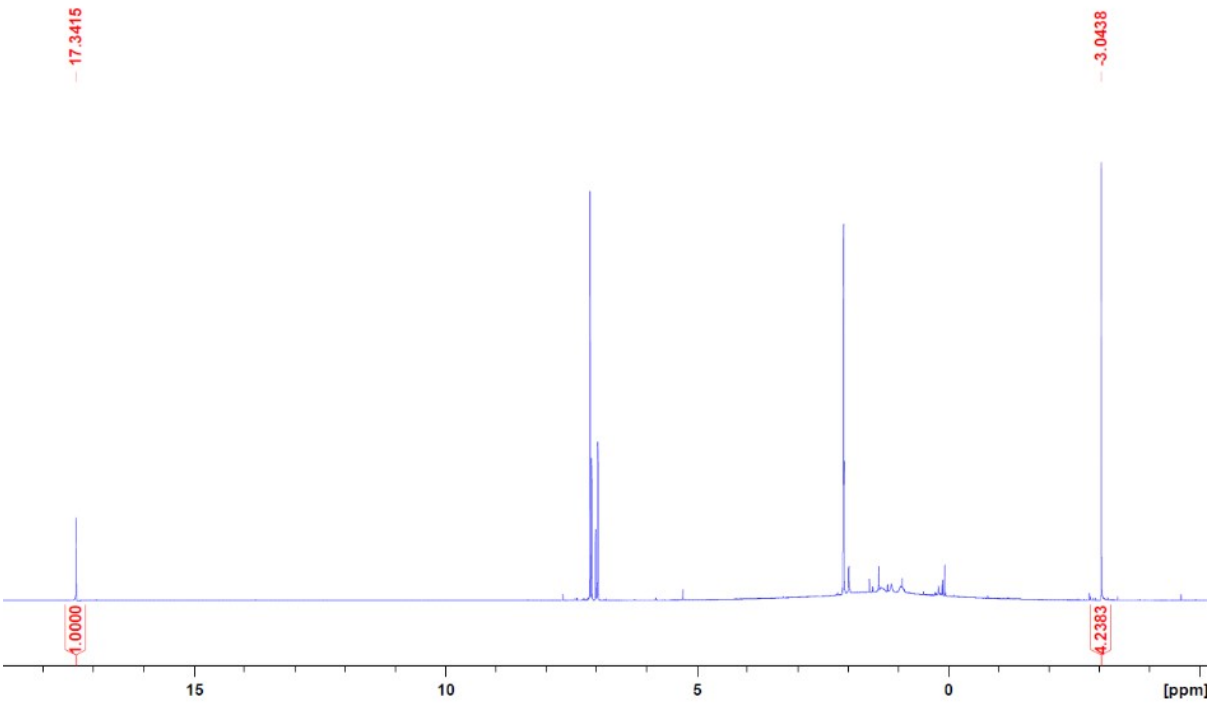

Figure S7 Paramagnetic ^{1}H NMR spectrum of [$UNa_2(O^tBu)_6$] (**UNa2**) in toluene-d_8 on a 500 MHz *Bruker Avance III 500* spectrometer.

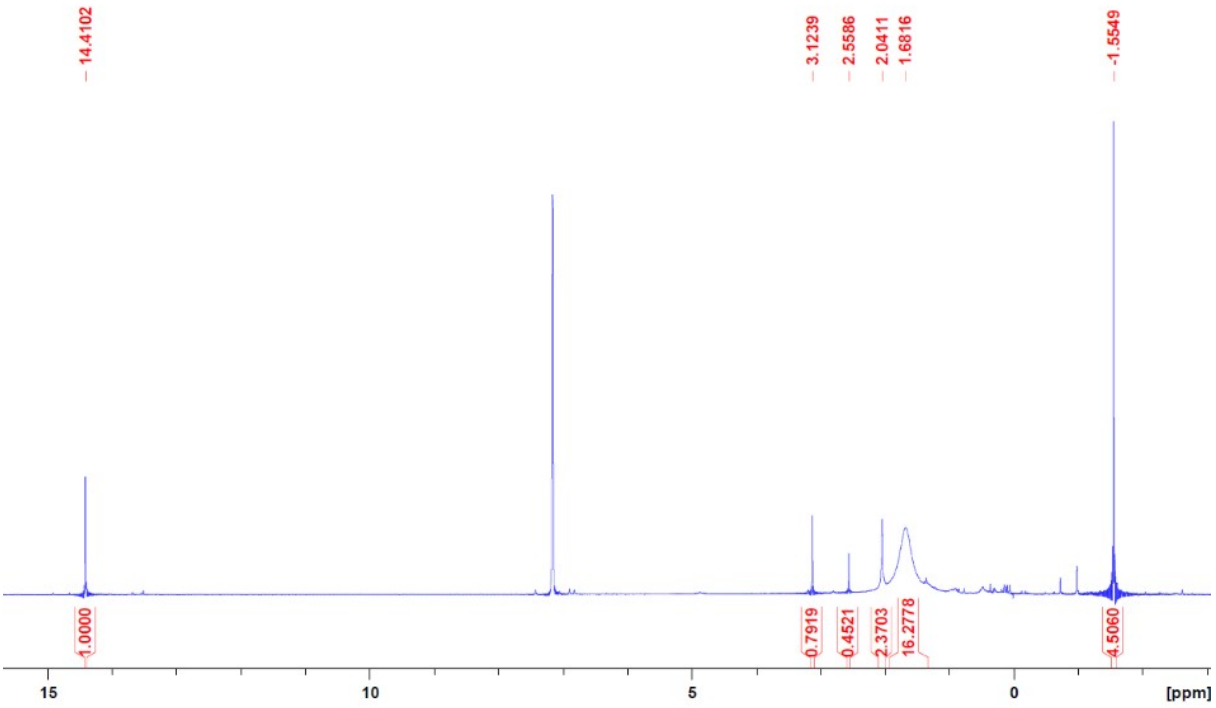

Figure S8 Paramagnetic ^{1}H NMR spectrum of [$UK_2(O^tBu)_6$] (**UK2**) in benzene-d_6 on a 300 MHz *Bruker Avance II 300* spectrometer.

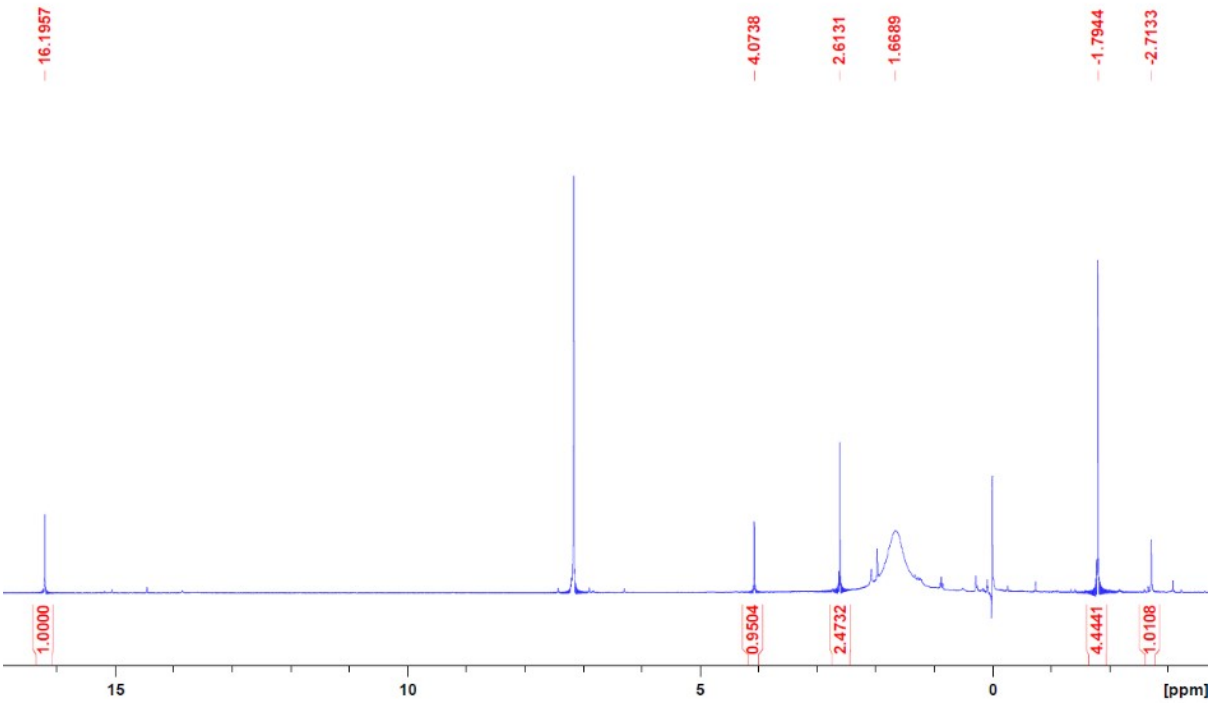

Figure S9 Paramagnetic ^{1}H NMR spectrum of [$URb_2(O^tBu)_6$] (**URb2**) in benzene-d_6 on a 300 MHz *Bruker Avance II 300* spectrometer.

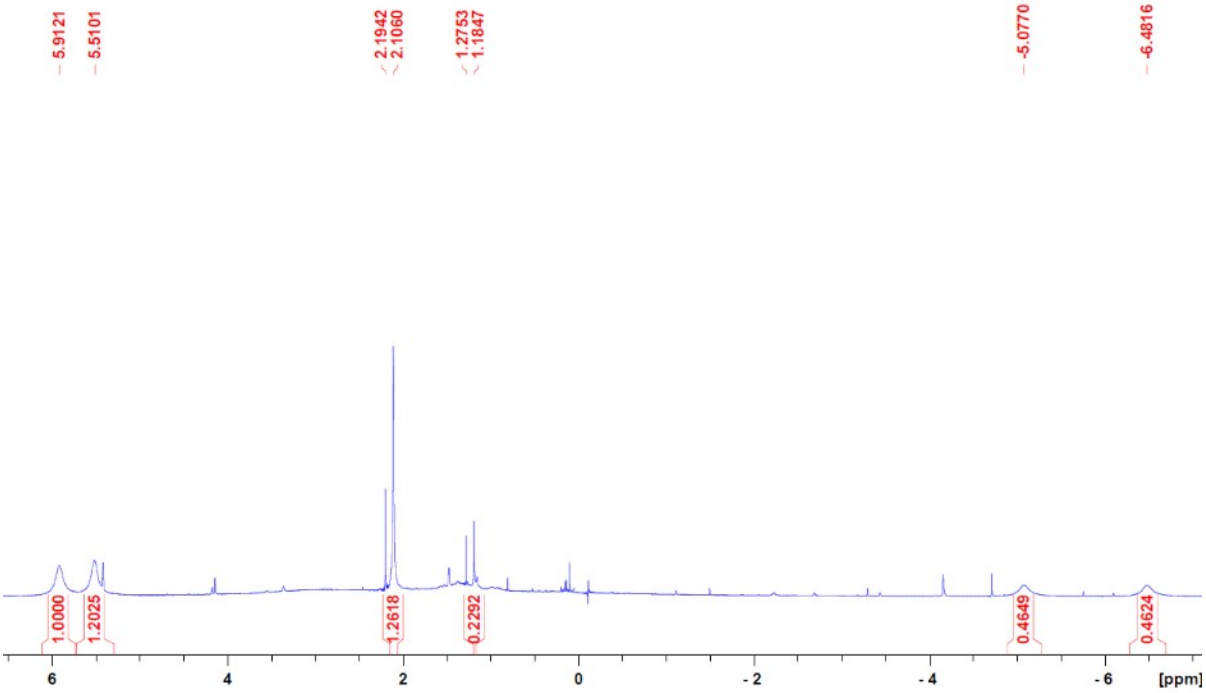

Figure S10 Paramagnetic ^{1}H NMR spectrum of [$UCs_2(O^tBu)_6$] (**UCs2**) in benzene-d_6 on a 400 MHz *Bruker Avance II 300* spectrometer.

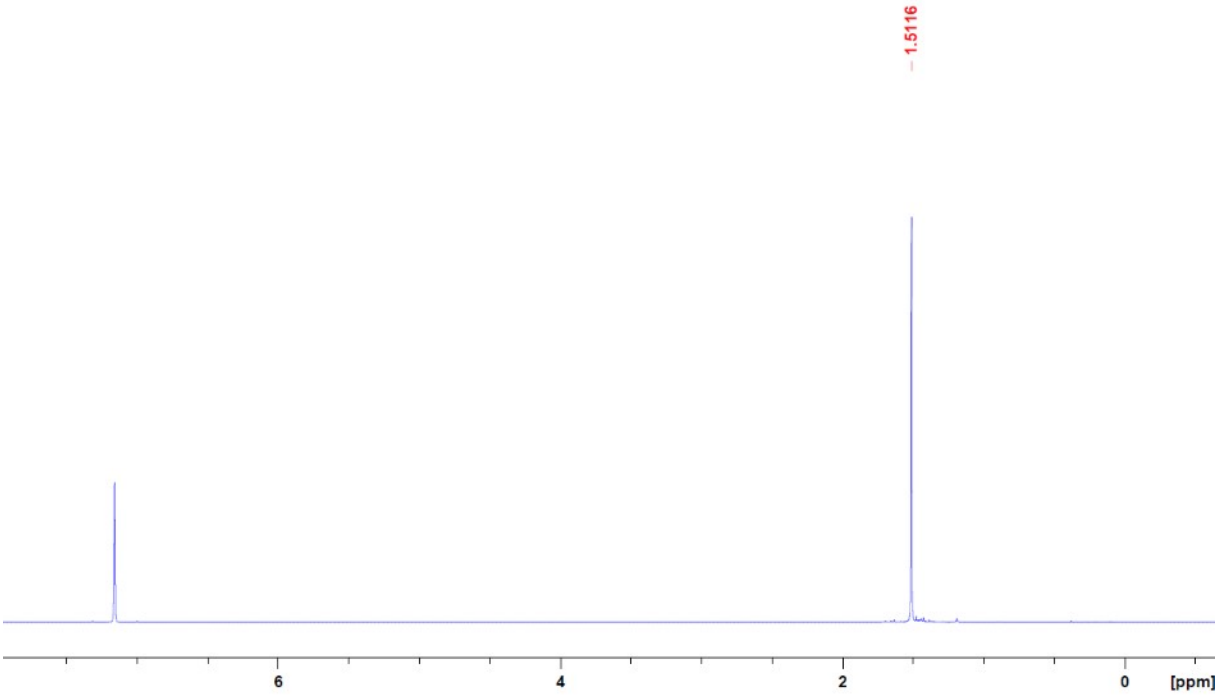

Figure S11 Diamagnetic ^{1}H NMR spectrum of [$ThK_2(O^tBu)_6$] (**ThK2**) in benzene-d_6 on a 300 MHz *Bruker Avance II 300* spectrometer.

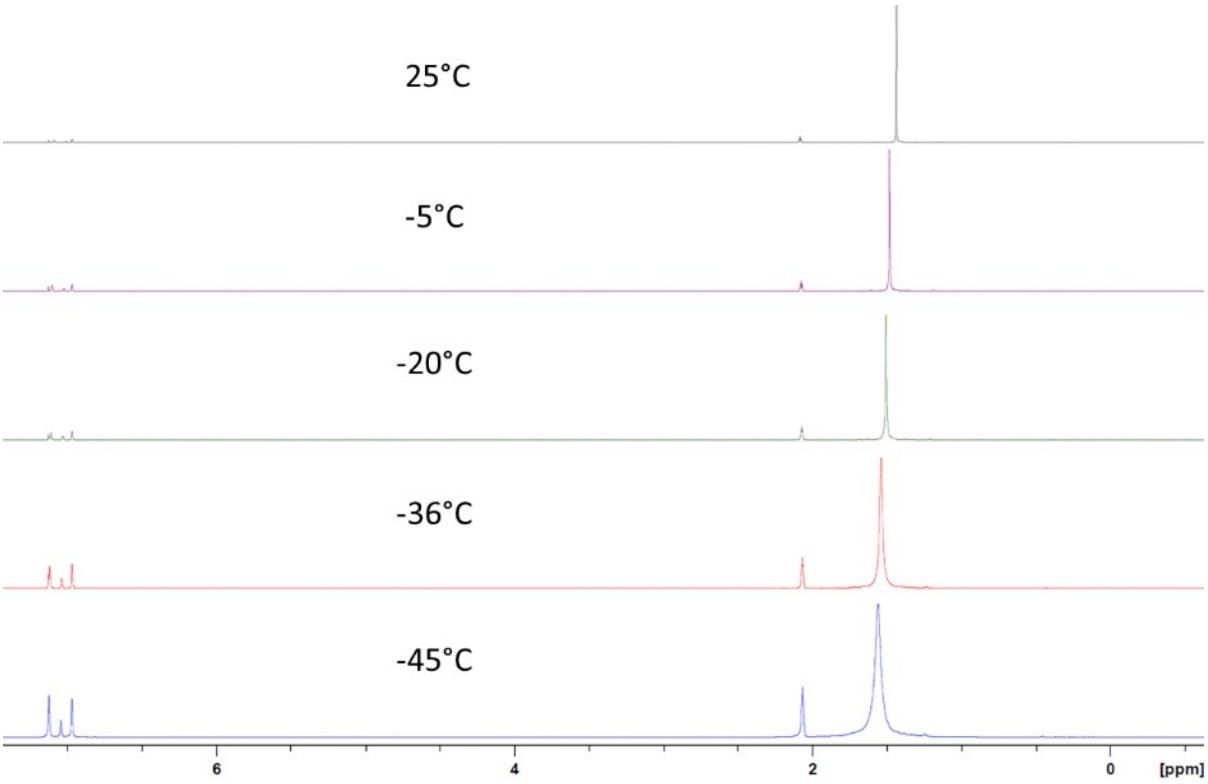

Figure S11-a Variable temperature (rt to -45 °C) 1H NMR of compound **ThK2** in tolouene-d_8 on 500 MHz *Bruker Avance 500* spectrometer.

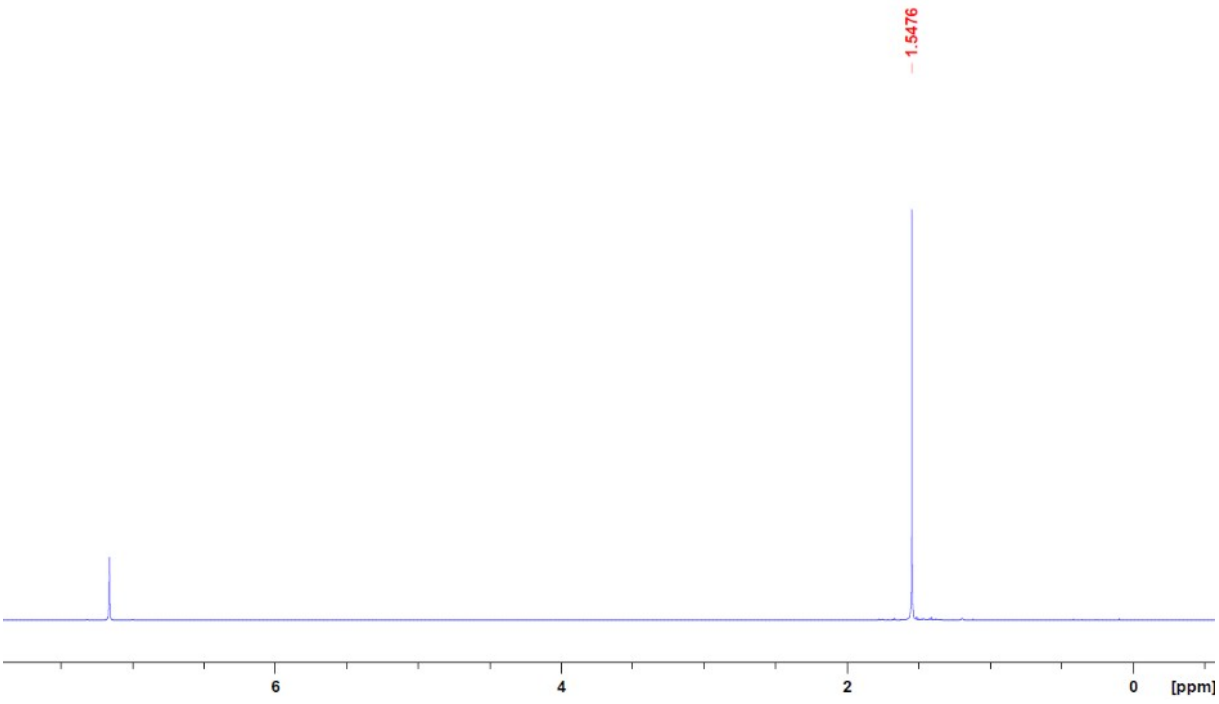

Figure S12 Diamagnetic ^{1}H NMR spectrum of [$ThRb_2(O^tBu)_6$] (**ThRb2**) in benzene-d_6 on a 300 MHz *Bruker Avance II 300* spectrometer.

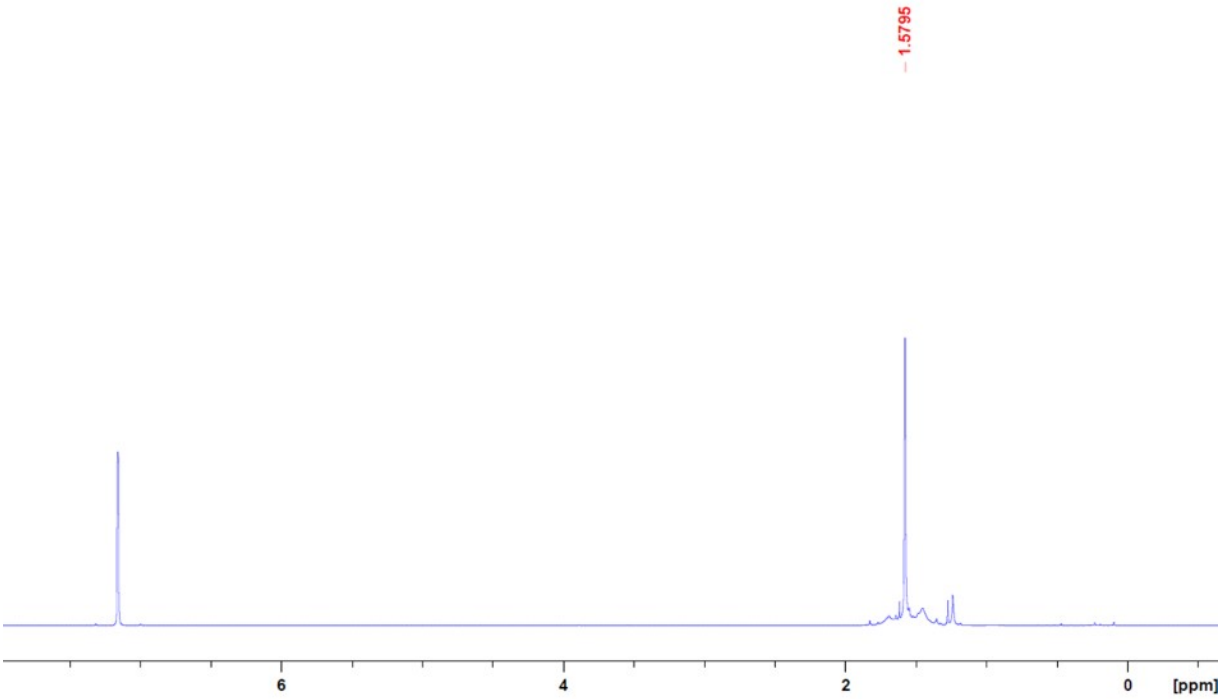

Figure S13 Diamagnetic ^{1}H NMR spectrum of [$ThCs_2(O^tBu)_6$] (**ThCs2**) in benzene-d_6 on a 300 MHz *Bruker Avance II 300* spectrometer.

Room temperature alkali metal isotope NMR

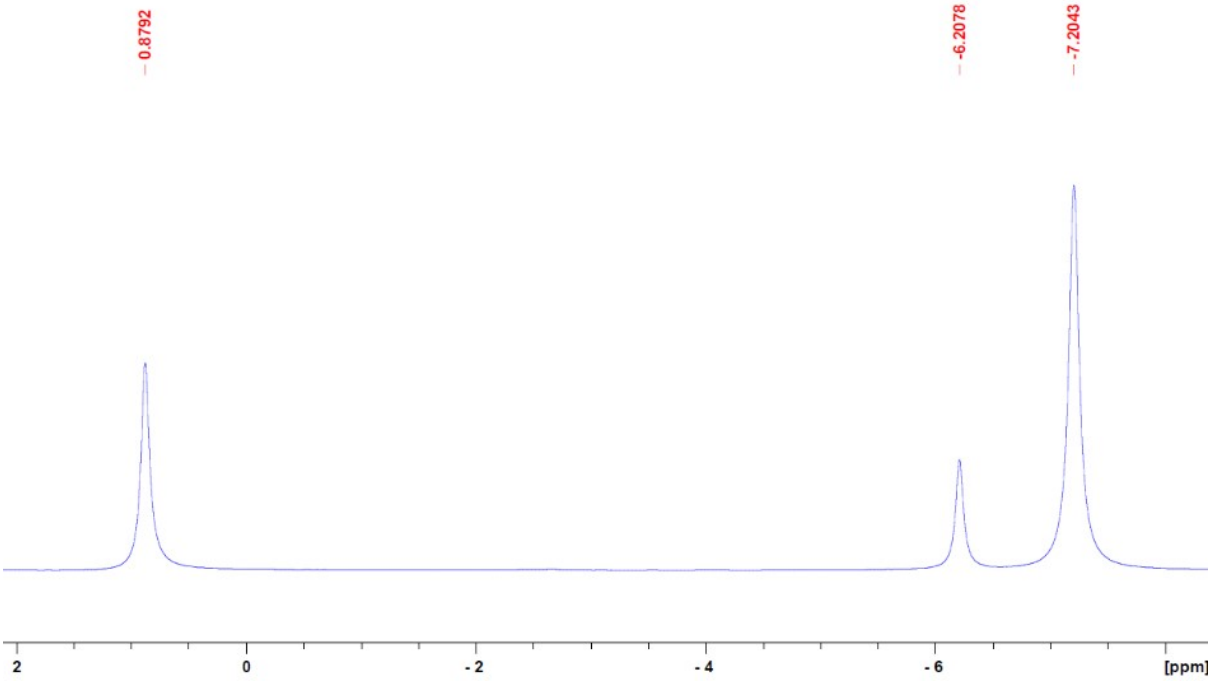

Figure S14 Paramagnetic ^{7}Li NMR spectrum of [$ULi_3(O^tBu)_7$] (**ULi3**) in benzene-d_6 on a 300 MHz *Bruker Avance II 300* spectrometer.

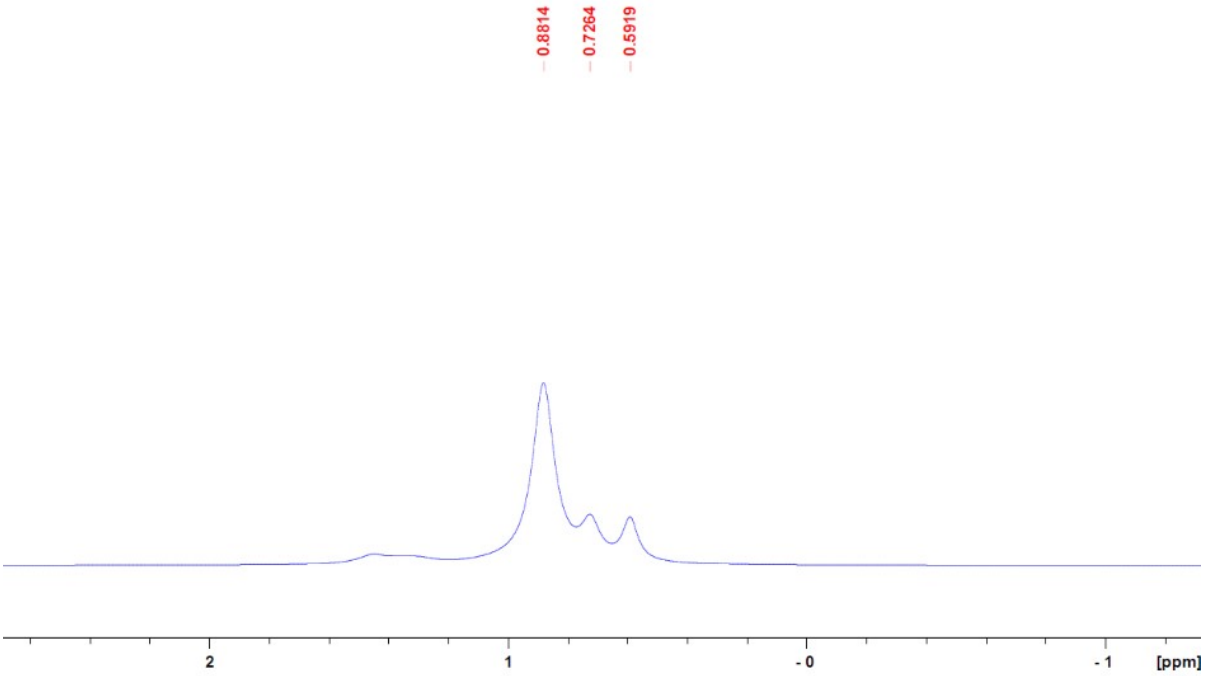

Figure S15 Diamagnetic ^{7}Li NMR spectrum of [$ThLi_3(O^tBu)_7$] (**ThLi3**) in benzene-d_6 on a 300 MHz *Bruker Avance II 300* spectrometer.

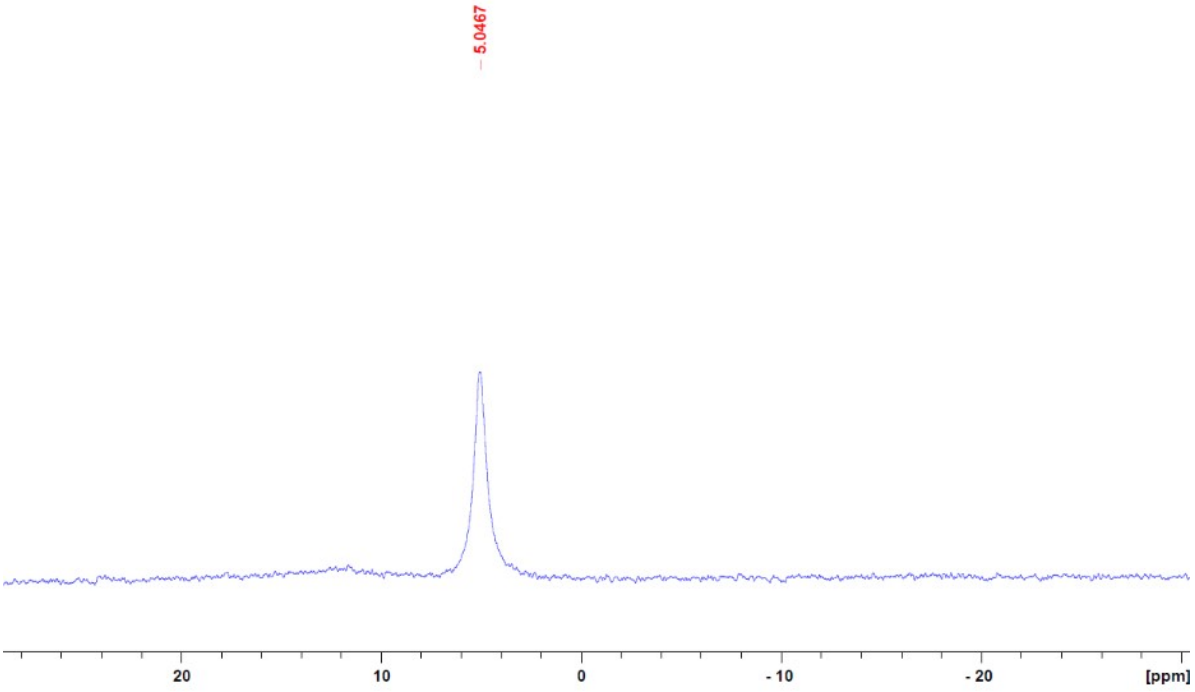

Figure S16 Diamagnetic ^{23}Na NMR spectrum of [$ThNa_3(O^tBu)_7$] (**ThNa3**) in toluene-d_8 on a 500 MHz *Bruker Avance 500* spectrometer.

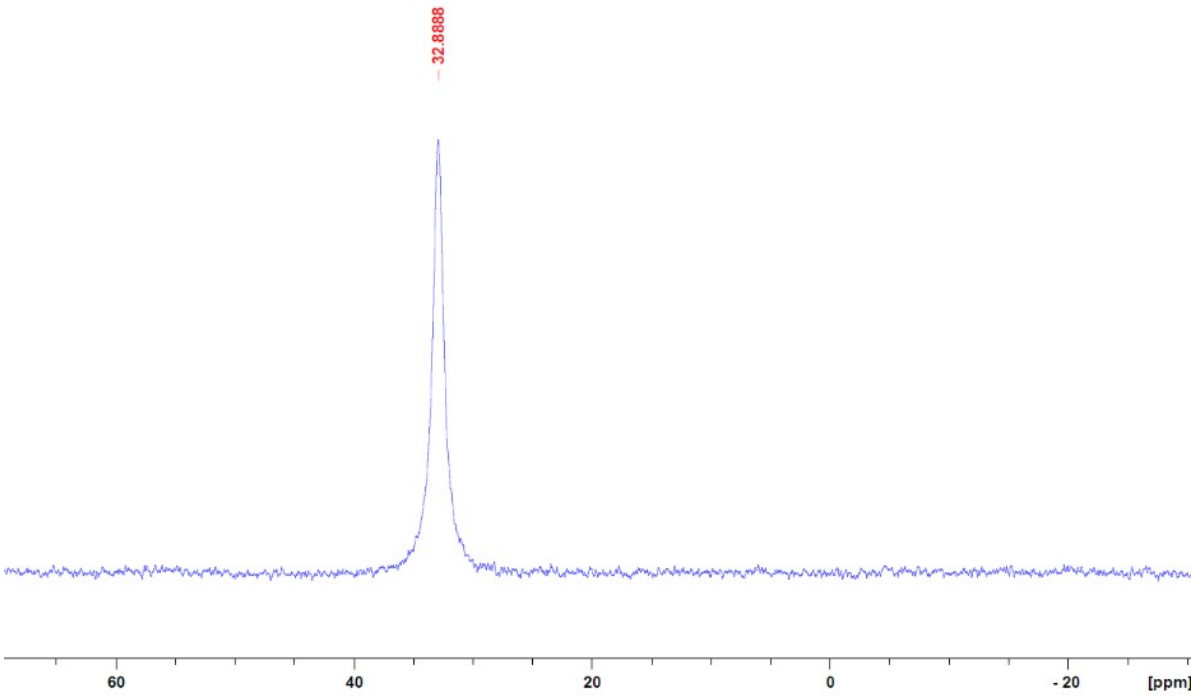

Figure S17 Paramagnetic ^{23}Na NMR spectrum of [$UNa_2(O^tBu)_6$] (**UNa2**) in toluene-d_8 on a 500 MHz *Bruker Avance 500* spectrometer.

Infrared spectroscopy

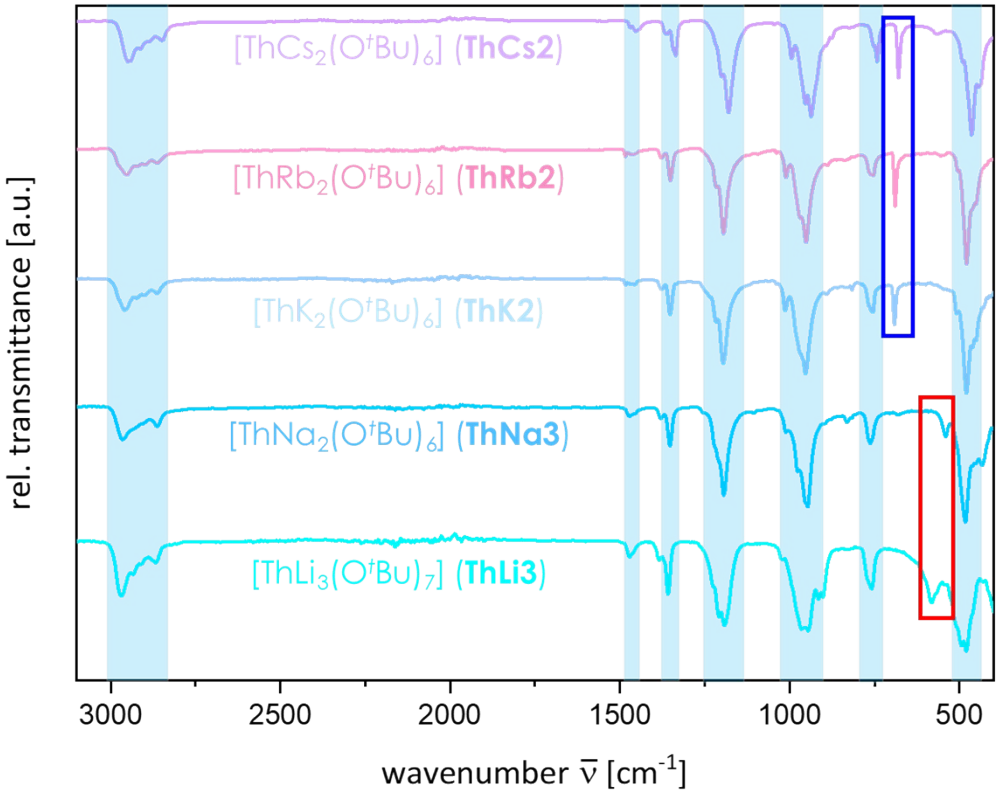

Figure S18 Infrared Spectra of the heterobimetallic $Th^{IV}M^{I}$ *tert*-butoxide compounds **ThM3** and **ThM2**.

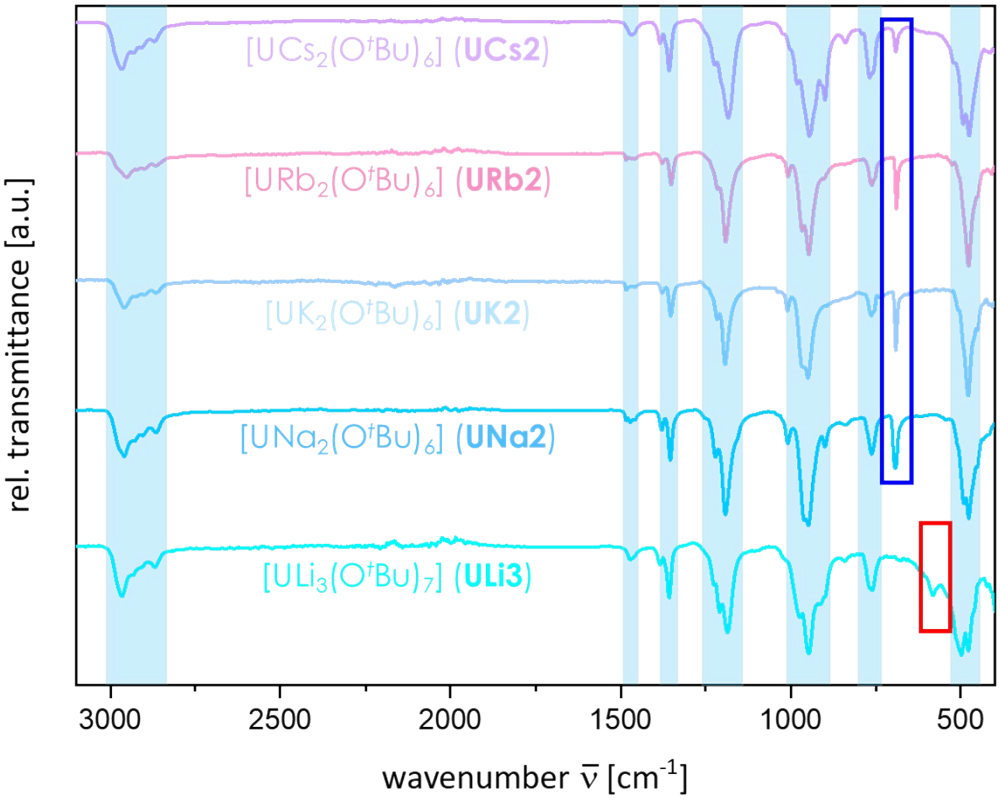

Figure S19 Infrared Spectra of the heterobimetallic $U^{IV}M^{I}$ *tert*-butoxide compounds **UM3** and **UM2**.

Additional Information

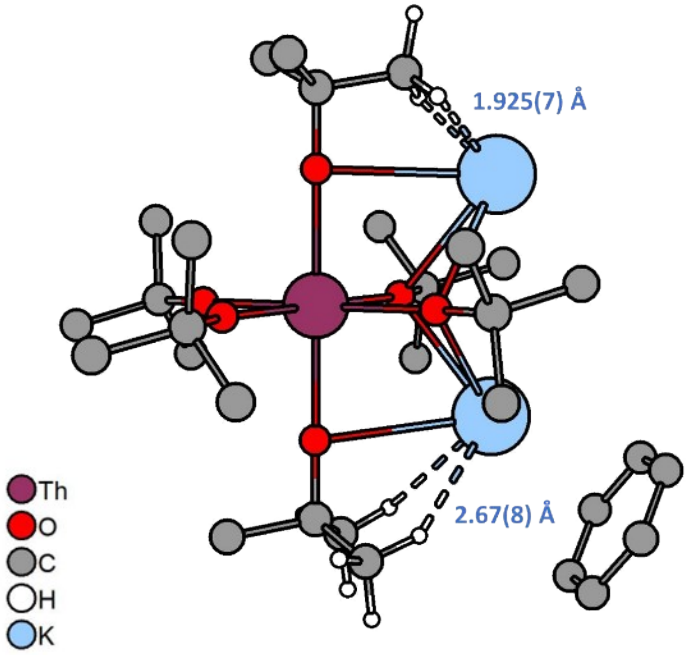

Figure S20 Molecular structure of ThK2. The dashed lines emphasize the agostic- and anagostic interactions between the hydrogen atoms of the methyl groups and potassium atoms. All other hydrogen atoms have been omitted for clarity.

Additional information for 1H NMR of ThNa3 compound

One explanation for the occurrence of only 2 singlet in the ratio (6:1) (**S5**) could be that the structure of ThNa3 in solution has a non-cubane framework that would differ from the solid-state arrangement. This could lead to a Na-Th bimetallic structure in which Th^{4+} is triply coordinated in a bidentate manner by two $[Na(O^tBu)_2]^-$ and one $[Na(O^tBu)_3]^{2-}$units, forming $[Th\{(\mu2\text{-}O^tBu)_2Na\}_3(O^tBu)]$ (see Fig. S21 **A**). Such a structure would generate two sets of signals for 6 ($\mu2\text{-}O^tBu$) bridging groups (red), which are chemically equivalent, and one terminal O^tBu group (blue). On the other hand, if this structure exists in the solution, then the Na NMR spectrum should show 2 distinct signals, one for the two chemically equivalent $[Na(O^tBu)_2]^-$ groups (pink) and one for $[Na(O^tBu)_3]^{2-}$ (green).

Since we observed only one Na singlet, which indicates that all three Na are chemically equivalent, we assume that the cubane structure obtained in the solid-state also exists in the solution state and that the two singletts of the terminal and bridging O^tBu groups coalesce. We have showed such similar coalescence of bridging- and terminal alkoxide groups in previous work reported from our group[2]. The low temperature measurement at -50 °C (tol-d_8) showed the appearance of additional singlet arising from a broad resonance in the range 1.36-1.99 ppm (see **S5a**) and a slight downfield shift of the resonance at 1.19 to 1.25 ppm. However, the relative intensities of the broad resonance and the singlet at 1.25 showed a ratio of (6:1), which underpins our observation and hypothesis.

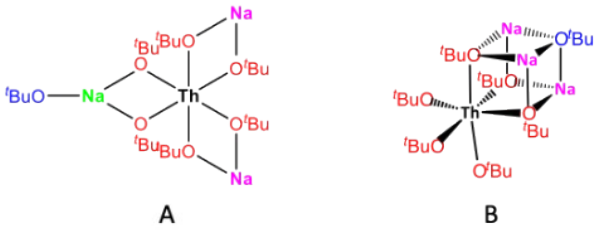

Figure S21 Molecular representation of Th and Na if two distinguishable Na resonances as well as different ^{t}BuO resonances were to be seen, which is NOT what we observe (**A**). In contrast, one single Na resonance indicates that the cubane-type structure (**B**) is retained even in solution.

Additional crystallographic information for URb2 (CCDC: 2152026)

This structure turned out to be more complicated than originally anticipated. Upon second inspection, regrowing the material and remeasuring the crystal as ALI280 we ran into several problems, particularly related to high residual electron density peaks around the heavy atoms. Face-indexed absorption corrections were performed but did not change the outcome.

A closer look at the low temperature data gave the following image in the lattice viewer of Apex, clearly indicating some reflections not attributable to the actual lattice.

Using strong reflections from the data set (or from the initial fast scan) they indexed as the same mono P unit cell (volume 3844). The frames look mostly clean, without any obvious twinning.

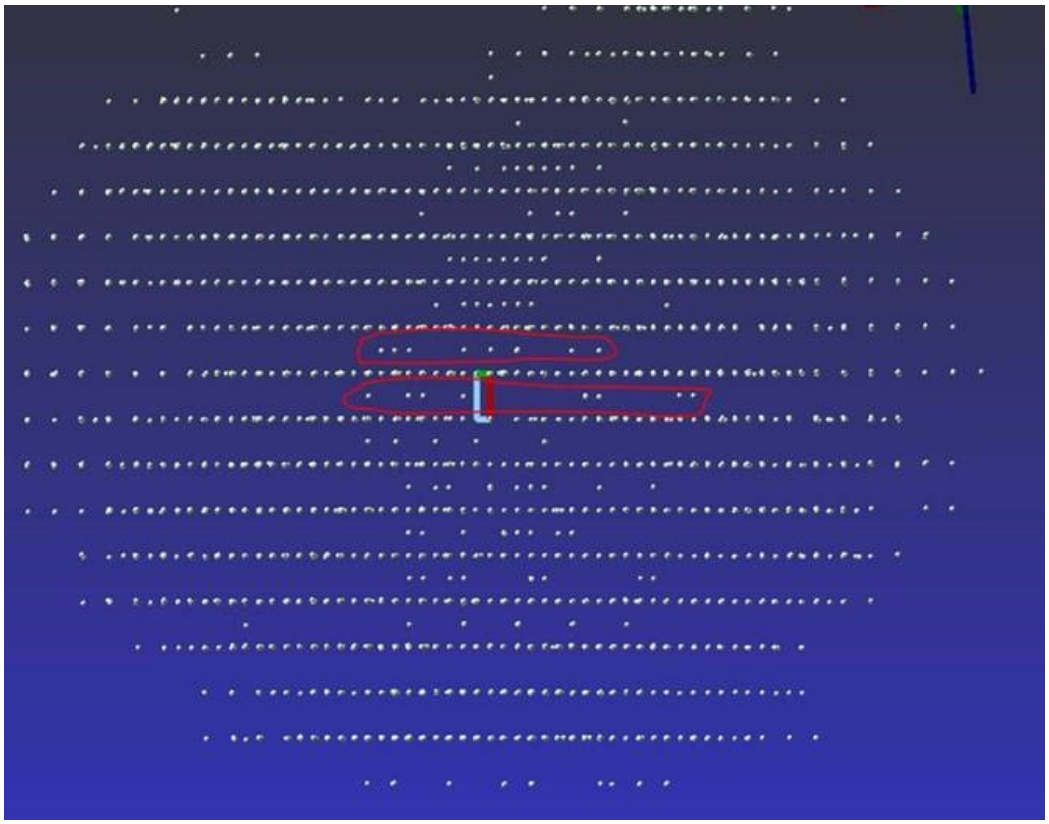

Figure S22 Additional reflections in RLATT which do not fit the unit cell, a first indication of a modulated structure.

One can see rows of unindexed reflections (some circled in red). Further harvesting reflections with an I/sigma cut off of 5 (in other words, including weak reflections), which is over 18,000 reflections in total gives a bigger unit cell with double the unit cell volume (12.66 32.70 19.49 90 107.3 90 V = 7703) and is still monoclinic. The reciprocal space plot shows more of the weak reflections, which are now indexed:

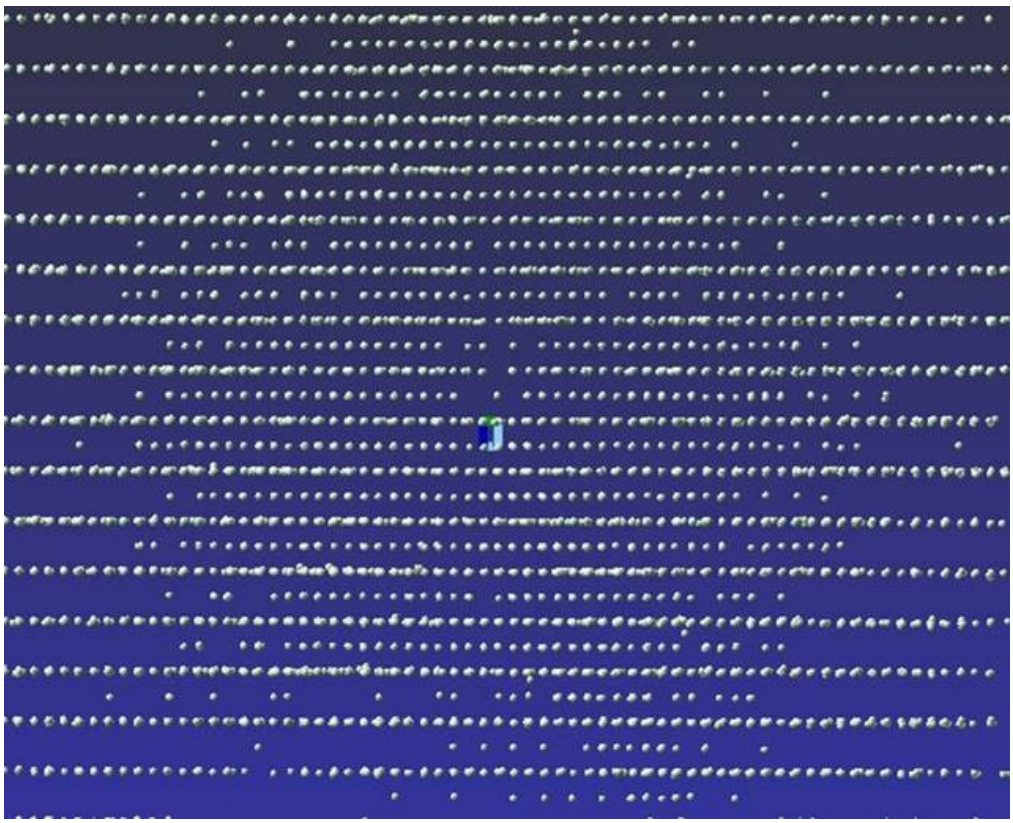

Figure S23 Weak reflections in RLATT with an I/sigma cut off at 5.

The data were then further integrated, scaled and tried to determine the unit cell. It's not unambiguous:

Systematic absence exceptions:

	-21-	-a-	-c-	-n-
N	150	2436	2482	2376
N I>3s	58	221	746	875
<I>	0.6	0.3	1.1	1.3
<I/s>	2.6	1.3	3.1	3.5

Identical indices and Friedel opposites combined before calculating R(sym)

Option	Space Group	No.	Type	Axes	CSD	R(sym)	N(eq)	Syst. Abs.	CFOM
[A]	P2	# 3	chiral	1	29	0.019	15455	0.0 / 1.3	30.69
[B]	P2/m	# 10	centro	1	21	0.019	15455	0.0 / 1.3	16.85
[C]	Pm	# 6	non-cen	1	1	0.019	15455	0.0 / 1.3	77.35
[D]	P2/c	# 13	centro	4	292	0.019	15455	1.3 / 2.6	11.82
[E]	Pc	# 7	non-cen	4	226	0.019	15455	1.3 / 2.6	26.97

Option [D] chosen

Here there are lots of weak systematic absence exceptions for the 21 screw axis and a-glide. They may be possibly related to those weak extra reflections. ShelXT finds three solutions in Pc, P2 and P2/c of which only the Pc solution looks like a molecule. It returned the same result. When forced to be P21/c the program finds no reasonable solution.

Attempting to integrate with a triclinic setting forced XPREP to pick P-1. XT reports two solutions, in P1 and P-1, neither of which are reasonable.

The crystal was then remeasured at room temperature, 200 K and 100 K, and the solution turned out to worsen with lowered temperature. Crystallographic advisors from Bruker who were consulted investigated this structure and were able to determine a modulation, which was strongest at low temperature. As this goes beyond the scope of the study, we did not ask our co-workers to model this modulation further. However, we used there structural solution of the room temperature data set as a proof of connectivity. For anyone interested our original data files are available through the Zenodo server where anyone may freely download them and model this system using the following link/doi: 10.5281/zenodo.7298626.

Below are the images of the 0kl and hk0 planes.

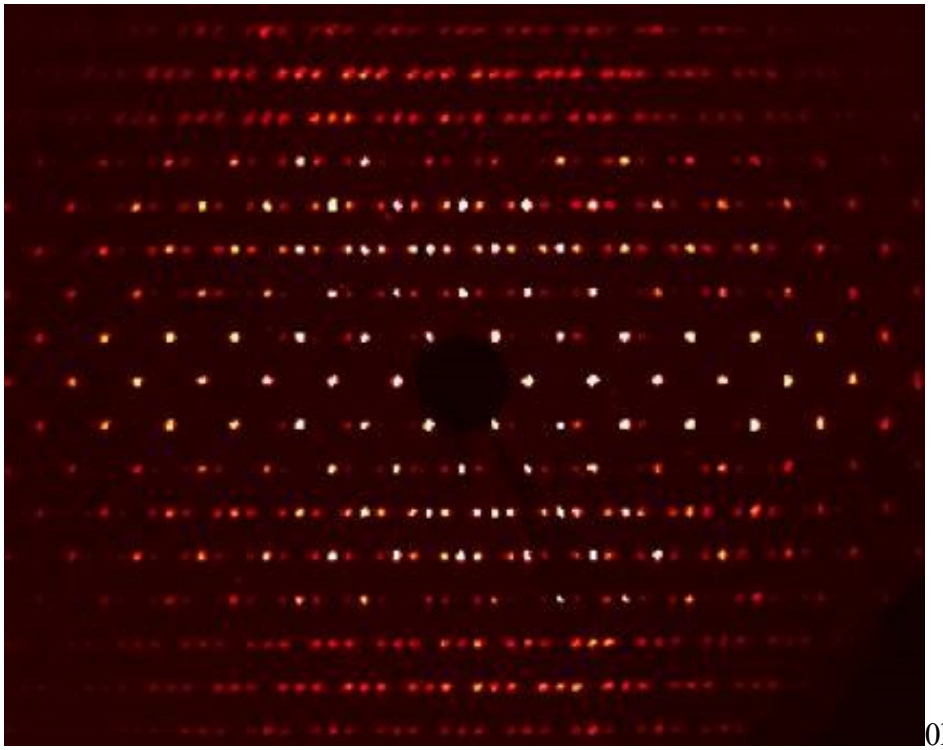
0kl

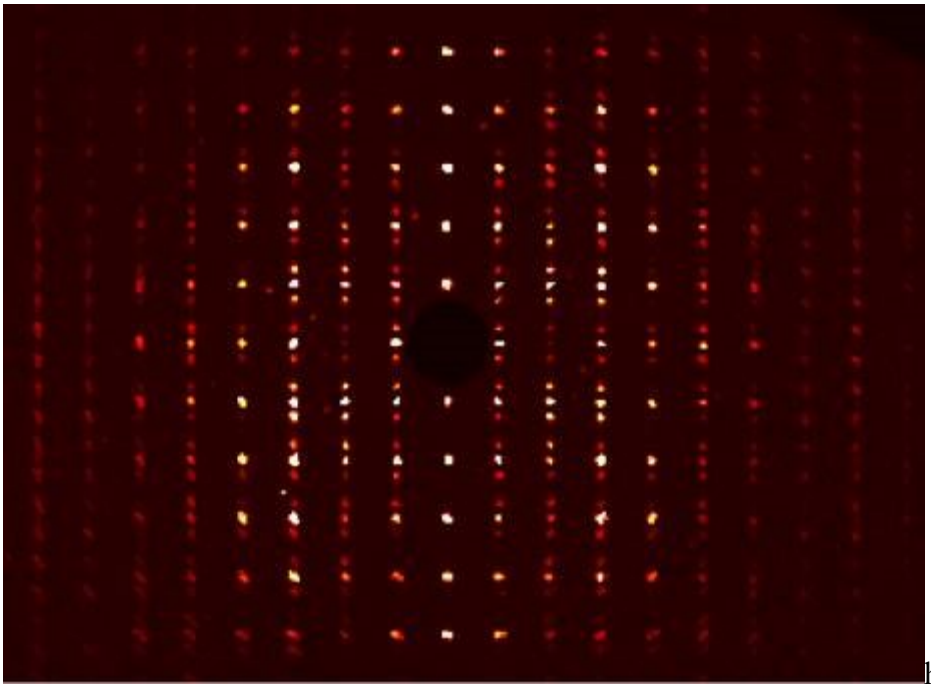
hk0

Figure S24 Images of the 0kl (top) and hk0 (bottom) planes indicating satellite reflections.

The following monoclinic primitive supercell can be used to describe all reflections:

9.8695 32.8160 12.8067 90.000 107.850 90.000

A closer look shows C-centering of a smaller subcell.

A proper description would be a (in)commensurately modulated monoclinic C-centered structure

12.8071 16.4117 9.8696 90.0000 107.8471 90.0000 (QVEC -0.00012 0.51951 -0.00006)

The following images shows the modulated average reflections (circles) and the respective satellite reflection (squares).

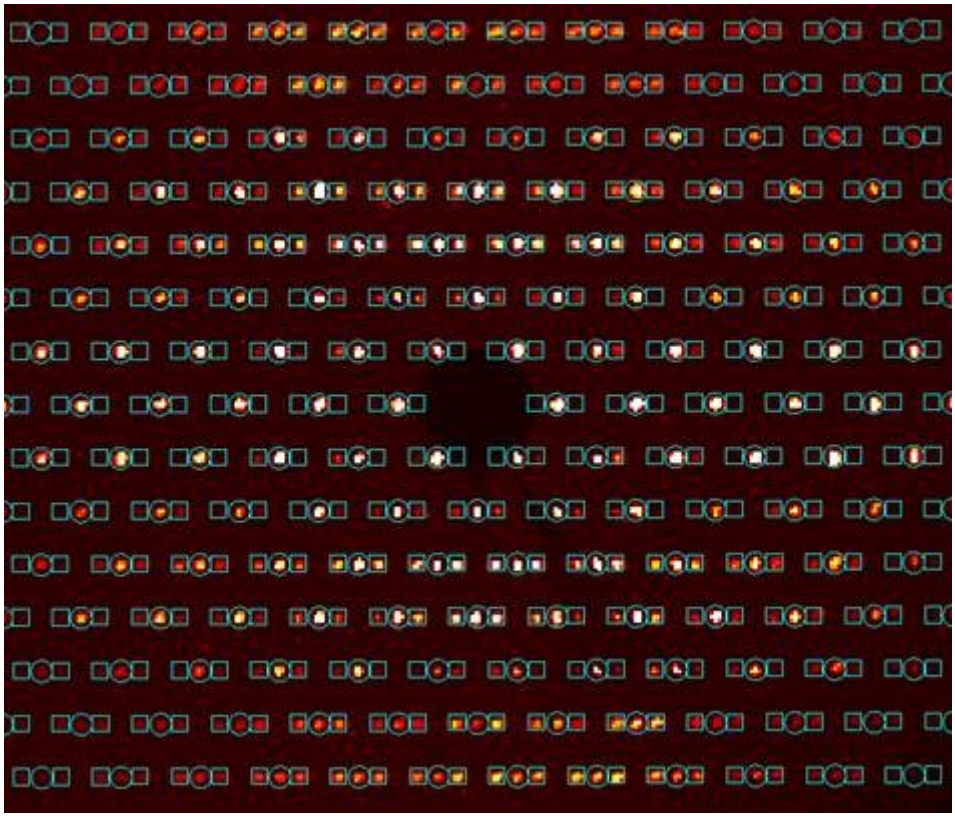

Figure S25 Modulated average reflections (circles) and the respective satellite reflection (squares).

An initial attempt to model this structure with Jana2020 needed more than two hours without coming to a reasonable final solution.

The full data set is accessible through Zenodo via the following link/doi:

10.5281/zenodo.7298626

Additional crystallographic information for ThNa3 (CCDC: 2152018)

Upon review of this manuscript the reviewer has requested to address the following crystallographic issues and provided us with some comments:

*"I apologize for not having been very clear here. Indeed, there are no CheckCif Alerts, but that does not mean that the structure is free of problems. In the attached map, it is clearly visible that Na1, O1 and C1 all appear to have been over-assigned. (and you would expect the sort of thing you see around the Th). If I refine the occupancy of Na1 freely, R1 will drop to 2.16% -- and the map around Na will be 'clean'. The Na will have an chemical occupancy of 0.72 (it is in a special position). O1 will also refine to 0.67, as well as C1 (0.65). This evidently doesn't make much sense here -- so the problem must be with your data (or, it *does* make sense, but I fail to see how. Maybe the cube *isn't* always there, but replaced by something else in ~70% of the cases?) At that point, there will be a very large residual peak of magnitude 4.5 -- *inside* the cube, and not associated with a metal. In any case, there are no weak reflections at all in the CIF file -- that is very odd -- and the name 'extension' of *_pl* is also somewhat ominous -- what has been done in PLATON with this? I hope you can see from the attached images why I can not recommend publication of this structure. Something is not quite right here. I am not trying to be difficult, but want to help out here -- this is a fascinating compound and it would be a shame if you ended up with troubles later on."*

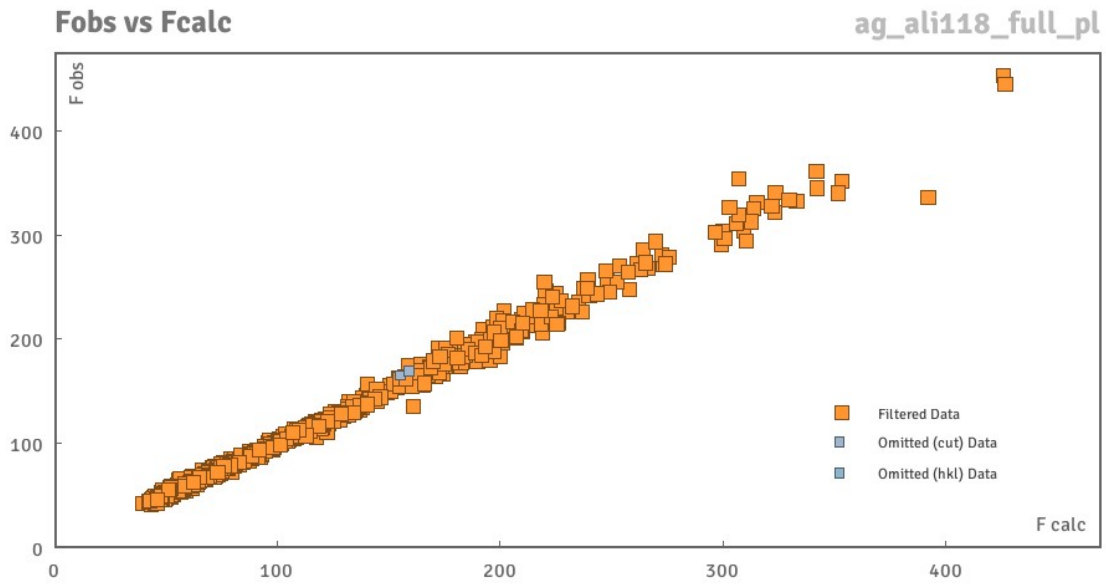

Figure S26 Fobs vs. Fcalc plot as provided by the reviewer before final corrections.

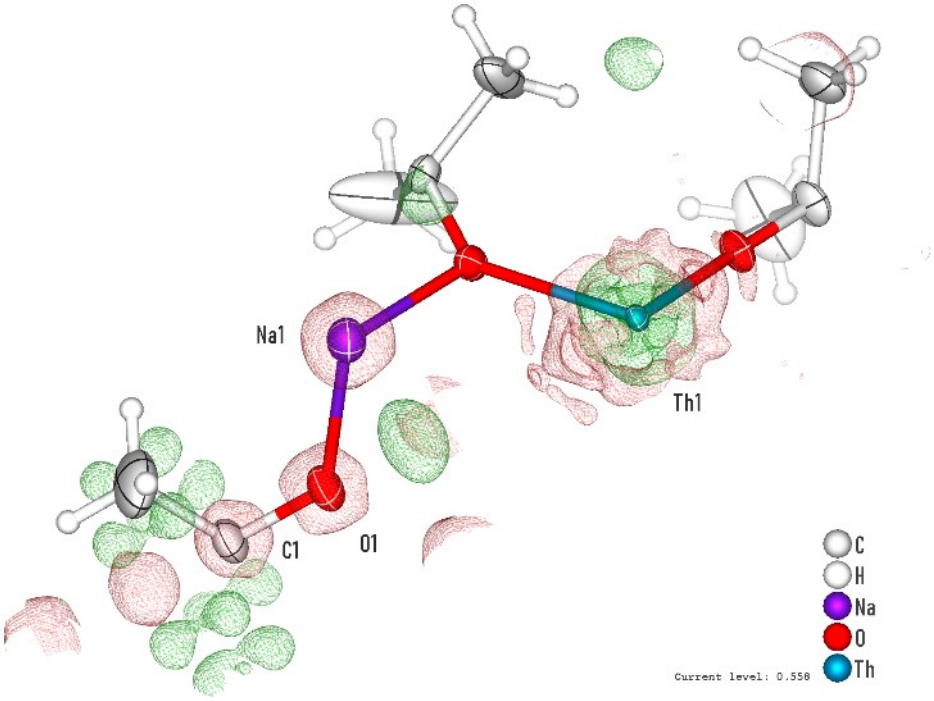

Figure S27 Electron density map as provided by the reviewer before final corrections.

In order to address this problem further we were provided with a preliminary solution by Carsten Lenczyk and Tobias Stürzer, who, however, were not able to address this problem any further. They instructed us to use this refinement as an inversion twin in R3 and address the positional disorder that they attribute to Na.

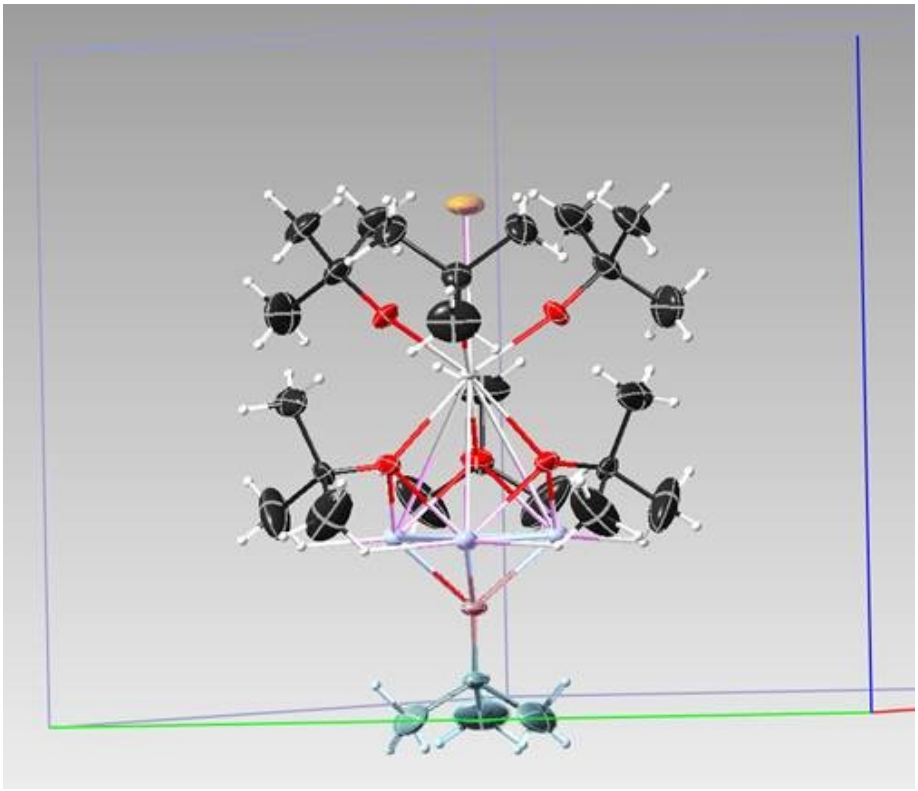

Figure S28 Initial refinement kindly provided by Carsten Lenzcyk and Tobias Stürzer.

Refining the structure with free occupancy on the Na atom and the attached t-butyl group leads to an occupancy of 0.685 for the respective atoms.

Along with this, another RED peak that sits on the molecular axis may be refined freely as another Na atom with an occupancy of 0.215, indicating a possible positional disorder.

However, such a refinement leads to a sum formula that makes chemically no sense and cannot be aligned with our other data. Modelling this structure further in such a way as to find RED that can be attributed to O and C atoms that ultimately result in a "complete" structural formula is not possible in our hands. The R1 of this refinement is 1.91%.

Refine the first and second Na atom with the respective second free variable results in an occupancy of the former of 0.706 and the latter of 0.294. However, as the former has a crystallographic occupancy of 1, and the latter of 0.33333, a sum formula of C26.8 H60.4 Na2.4 O6.7 Th results. A total of 2.4 sodium atoms is not in accord with the charge balance and our other data. The max peak is now 1.5 while the min peak is -1.4, which makes it hard, if not impossible to search for RED that could be attributed to the remainder of the Na electron density to sum up the formula to three sodium atoms. The R1 is still 1.91%.

This solution comes probably reasonably close to crystallographic satisfaction, however, chemically this is not an adequate model.

In order to come to a chemically reasonable model we refined the C and O atoms with full occupancy instead of free (0.74). Doing that results in a sum formula of C28 H63 Na2.4 O7 Th and changes R1 to 1.93%.

However, in order to address the sum formula with respect to the sodium ions, we found that these are not depending on each other, so we refined Na2 freely, and matched the occupancy of Na1 in such a way that the sum formula is now C28 H63 Na3 O7 Th. R1 has decreased slightly to 2.11%, which we believe at this stage is justifiable and representing the structure as well as possible.

The full data set is accessible through Zenodo via the following link/doi:

10.5281/zenodo.7432752

Additional crystallographic information for ThCs2 (CCDC: 2152020)

Upon review of this manuscript the reviewer has also requested us for this structure to address the following crystallographic issues and provided us with some comments:

*"Ok -- I don't know what causes these data issues -- but refining the EXTInction here is certainly not appropriate. The I/σ(I)P maybe has a hint: how can this plot have a *maximum* that is not right over at the low-angle side? This seems to suggest that strong (or at least low-angle) reflections have been measured significantly worse than higher angle reflections. Again, this is probably a problem with the data reduction. The Rint plot follows this trend also. The effects of all of this are pretty severe -- a max|min of 3.0|-4.6 and a GooF of 1.357 clearly spell out trouble."*

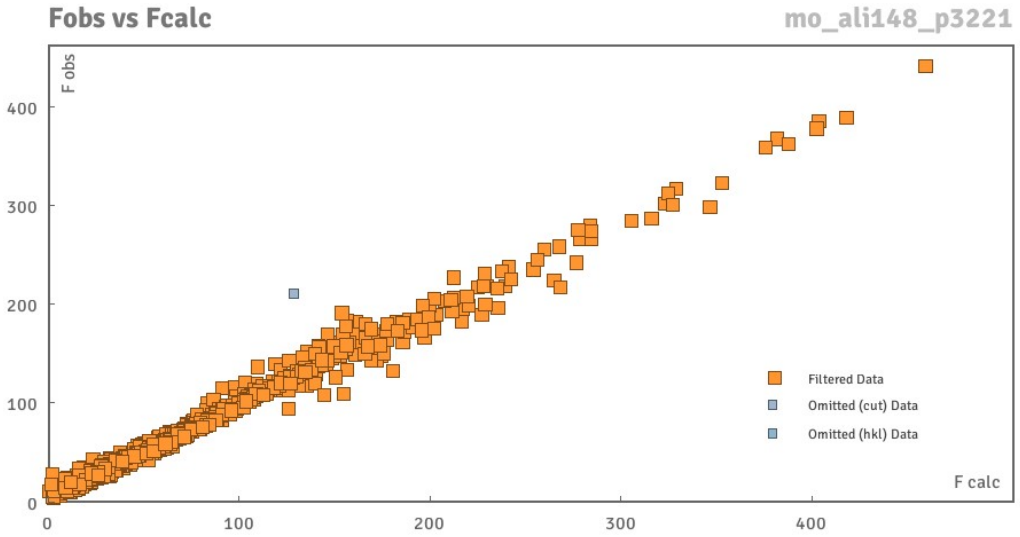

Figure S29 Fobs vs. Fcalc plot as provided by the reviewer before final corrections.

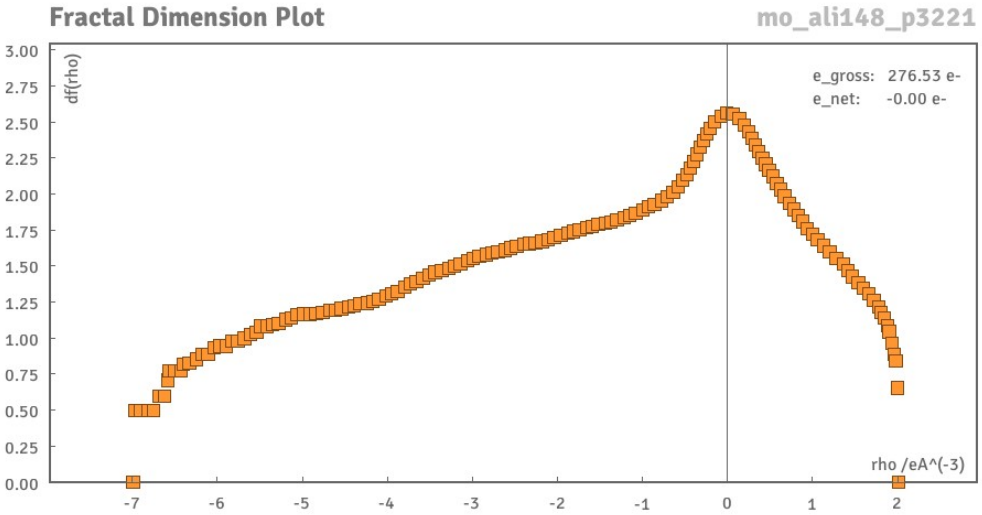

Figure S30 Fractal dimensions plot as provided by the reviewer before final corrections.

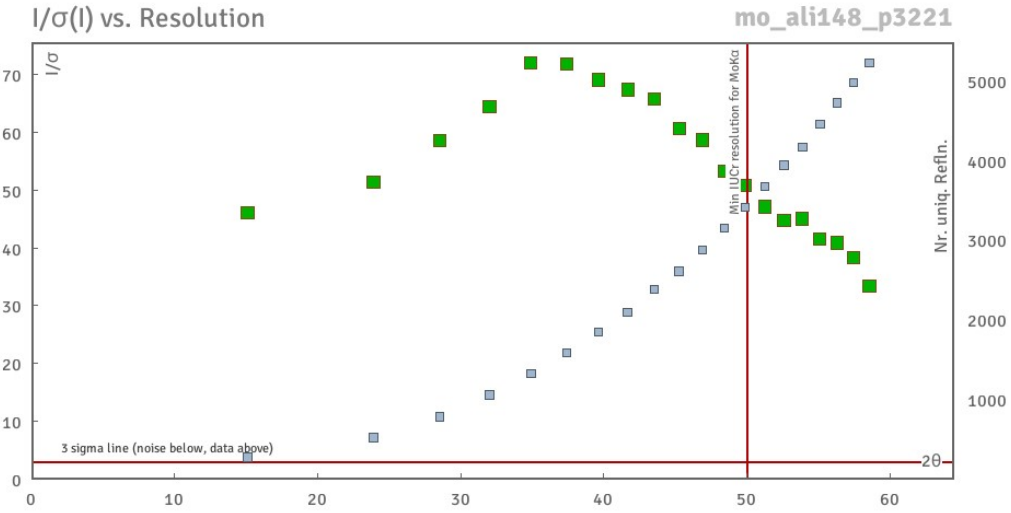

Figure S31 I/σ(I) vs. Resolution plot as provided by the reviewer before final corrections.

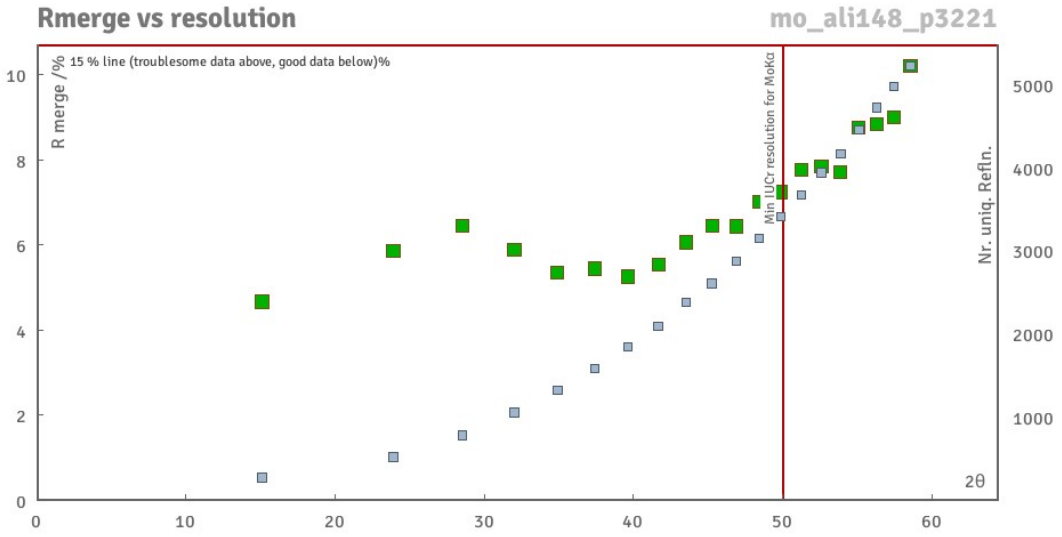

Figure S32 Rmerge vs. resolution plot as provided by the reviewer before final corrections.

For this structure we were provided with a model refined as a merohedral twin in P32 by Carsten Lenczyk and Tobias Stürzer, that now refines to an R1 of 3.77%, a max peak of 2.2. and a min peak of -4.0 with a GooF of 1.129.

This is as much of an improvement as we could possibly obtain.

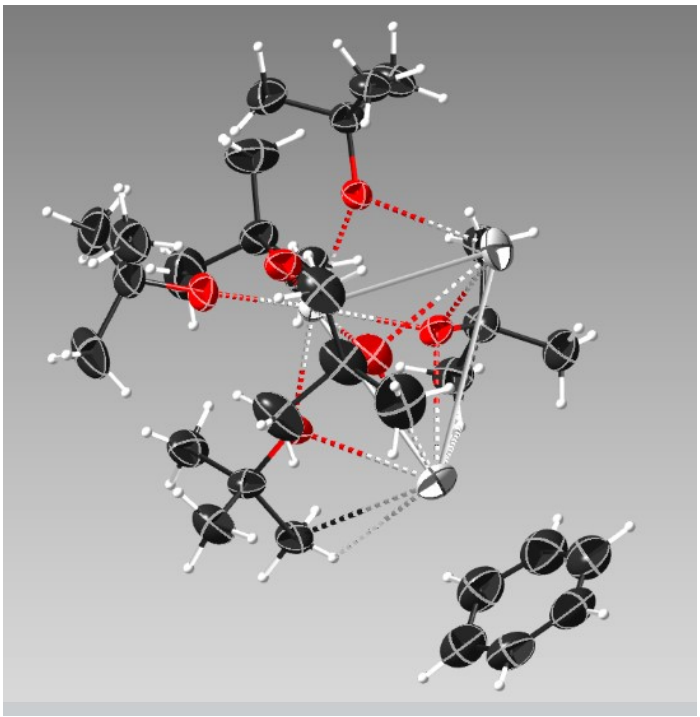

Figure S33 Merohedral twin model kindly provided by Carsten Lenczyk and Tobias Stürzer.

When checking the packing in the cell there is quite a bit of empty space around the Cs atoms.

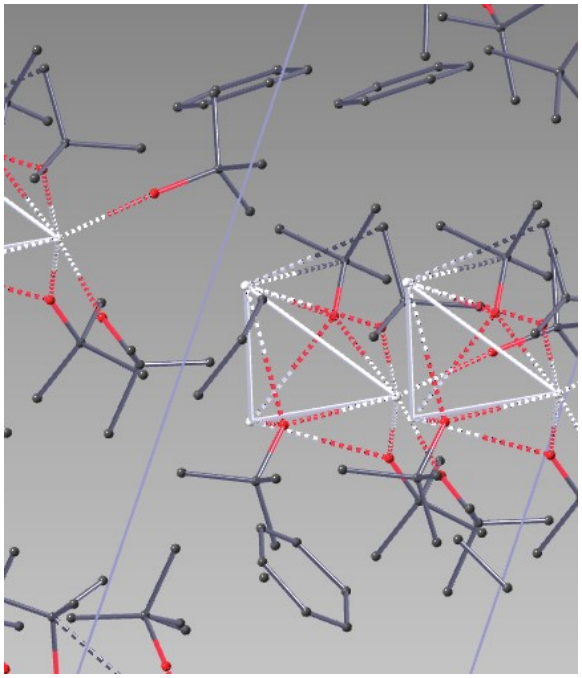

Figure S34 Packing in the model by by Carsten Lenczyk and Tobias Stürzer.

However, when running platon Solv it is still OK.

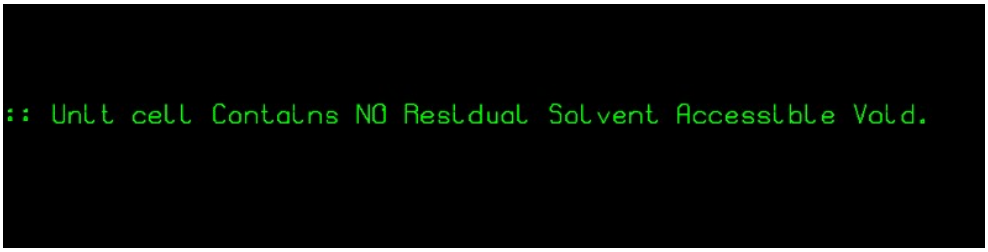

Figure S35 Platon output.

Regarding the voids, these seem to be a crystallographic feature, even though Platon does not seem to find any.

The full data set is accessible through Zenodo via the following link/doi:

10.5281/zenodo.7432503

References:

1. Fortier, S.; Wu, G.; Hayton, T. W., Synthesis and Characterization of Three Homoleptic Alkoxides of Uranium:[Li (THF)] 2 [UIV (O t Bu) 6],[Li (Et2O)][UV (O t Bu) 6], and UVI (O t Bu) 6. *Inorganic chemistry* **2008,** *47* (11), 4752-4761.
2. Jamil, A.; Schlafer, J.; Gonullu, Y.; Lepcha, A.; Mathur, S., Precursor-Derived Rare Earth Metal Pyrochlores: Nd2Sn2O7 Nanofibers and Thin Films As Efficient Photoabsorbers. *Cryst Growth Des* **2016,** *16* (9), 5260-5267.